HYDRODYNAMIC SHEAR BREAKAGE OF NATIVE DNA

Thesis by

Ray Douglas Bowman

In Partial Fulfillment of the Requirements

For the Degree

Doctor of Philosophy

California Institute of Technology

Pasadena, California

1971

(Submitted March 19, 1971)

To my father

ACKNOWLEDGMENTS

I gratefully acknowledge the guidance and inspiration given me by my thesis advisor, Norman Davidson. I have profited considerably from his keen insight into physical chemistry and from his articulate manner of describing scientific concepts.

I would like to thank Professors Alan Hodge, James Bonner, and the late Jean Weigle for allowing me unrestricted use of their respective analytical ultracentrifuges. I would especially like to thank Professor Jerome Vinograd not only for helpful technical advice and generous loans of equipment, but also for the encouragement and sense of perspective which his discussions with me invariably generated.

There are many more people to whom I am indebted for helpful advice and instruction during my graduate work. I will only mention here those whose efforts in my behalf became part of the data for this thesis. These are William Anthony, Chong Sung Lee, Douglas Mohr, Martha Simon, and Professor Donald Cohen.

I am grateful for the financial support of the predoctoral Traineeship given me by the U. S. Public Health Service.

ABSTRACT

Shear breakage is the process by which high molecular weight polymers are broken one or more times by shear stress generated in liquid velocity gradients. This thesis is a kinetic study of the breakage of native DNA from the coliphage $\lambda b_2 b_5 c$ (contour length 12.8 μ) in dilute aqueous solution. Breakage of this DNA is produced by flow through a capillary. In all our experiments, each DNA molecule breaks only once to form two approximately half-sized molecules. The shear stress required to induce breakage is about 10^3 dynes/cm^2. We find that the kinetics of breakage are first order and that the first order rate constant is a function of the fifteenth power of the shear gradient at 25°C. The shear stress required to produce breakage at a particular rate increases linearly with DNA concentration over the range 0.05 μg DNA/mℓ to 7.5 μg DNA/mℓ. We observe a very large temperature coefficient for the breakage rate which arises from the effect of temperature on the viscosity of the DNA solution. This result indicates that the rate limiting step for DNA shear breakage is the speed at which random coil DNA unfolds to an extended configuration when it enters the capillary's liquid velocity gradient. We discuss a kinetic model and a simple theoretical model which have properties similar to those observed experimentally.

TABLE OF CONTENTS

INTRODUCTION

An interesting and unusual property of large native DNA molecules is that they can be broken near their midpoints by hydrodynamic shear stress. A long rodlike molecule in a liquid velocity gradient tumbles as it moves with the liquid; while tumbling, it is alternately compressed and stretched along its major axis. The tensile force reaches a maximum near the center of the molecule, and if the liquid velocity gradient is large enough, the force can rupture covalent bonds. High molecular weight DNA is a wormlike coil, not a rigid rod. Such a threadlike molecule engages in all sorts of gyrations--bending and stretching motions--as it tumbles in a shear field, but there still are tensile forces tending to break the molecule in the middle.[1]

This thesis reports a study of the kinetics of hydrodynamic shear breakage of native DNA and of the effects of several variables thereon. The variables whose effects are measured are shear stress, viscosity, temperature, salt concentration and DNA concentration. No consideration is given to the effects of DNA molecular weight or base composition. Native DNA from the coliphage $\lambda b_2 b_5 c$ (molecular weight 25×10^6 daltons) was used exclusively in this work.

Shear breakage of DNA became of interest in molecular biology when investigators reported different molecular weights for DNA from the same source. Peter Davison,[2] and A. D. Hershey and Elizabeth Burgi[3] were among the first to show that DNA from several

bacteriophages could be broken by shear gradients generated in the course of handling DNA solutions in the laboratory.

Historically, there have been numerous studies of DNA breakage by hydrodynamic shear.[2-14] Some devices used to generate liquid velocity gradients of sufficient magnitude are sonicators, syringe needles, an atomizer, capillaries and a piston and cylinder apparatus. The most common device used to shear DNA is a laboratory homogenizer. We chose capillaries for our study because they are easily constructed and their flow characteristic are accurately known. Pressurized nitrogen gas is the driving force for pushing DNA solutions back and forth through the capillary. An electro-optical system, which senses liquid levels in the device, triggers the valves controlling the nitrogen and makes the apparatus completely automatic.

Our approach to hydrodynamic shear breakage was influenced primarily by the work of Levinthal and Davison.[4] They estimated the force exerted on T2 DNA by capillary flow and compared it to calculated bond strengths of the DNA backbone. The hydrodynamic model for DNA they thought relevant was a rigid rod which at some time becomes oriented at 45° to the liquid flow lines. They showed the maximum tensional force on such a molecule is proportional to the shear stress, ηG, and is dependent on the square of the length of the rod.

We wished to investigate whether DNA shear breakage is a mechanical process--the shear stress just rips the bonds apart--or

whether it is a mechanically assisted solvolysis--the mechanical forces serve to stretch bonds and to facilitate thermal solvolysis. Other workers had shown prior to the beginning of our study that DNA breakage proceeds primarily by 3′C–O bond cleavage.[15,16] We worked on the hypothesis that breakage was a mechanically assisted hydrolysis and set out to demonstrate the existence of a temperature coefficient for the reaction. We believed that the activation energy for the breakage reaction at constant mechanical tension should be calculated from the temperature coefficient at constant shear stress of the reaction rate constant, specifically,

$$\Delta H_{act} = R\left(\frac{d\,\ell n\,k}{d(1/T)}\right)_{\eta G} .$$

As we shall see, this point of view is not consistent with the final results. We find that there is a very large temperature coefficient for DNA shear breakage at constant shear stress, but this does not arise from the influence of temperature on a thermal reaction. It is instead due to the fact that at constant shear stress, there is a very marked effect of solvent viscosity on the breakage rate. The temperature coefficient is simply due to the effect of temperature on viscosity. We have concluded that the rate limiting step in DNA shear breakage is the rate at which the molecules unfold to extended configurations upon entering the capillary flow field.

EXPERIMENTAL

Breakage Apparatus

The shear breakage capillary, shown in Figure 1, consists of a precision bore capillary connected on either side by means of larger bore capillary tubing to two reservoirs of thick walled glass tubing. Each reservoir is connected to a three way solenoid valve by flexible stainless steel tubing. Pressurized nitrogen gas drives the solution back and forth through the capillary. As the meniscus in the pressurized reservoir descends to its lowest point, it intersects a light beam issuing from an optic fiber scanner (light pipe). The signal generated causes the opposite reservoir to be pressurized and the direction of the solution to be reversed.

Periodically during an experiment, the flow was stopped and a sample of sheared DNA was withdrawn. These samples were typically 0.15 ml. The total volume of the solution was typically 10 ml.

Three capillaries were used for the experiments reported in this thesis. Their dimensions and other relevant characteristics are given in Table I. The capillary tubing was precision bore Pyrex glass capillary; all other glass materials were stock Pyrex.

Nitrogen pressure was measured with Marshaltown Permagages and regulated by a Harris multistage regulator. The pressure was reproducible within 1% and was constant during an experiment within 2%.

The capillary apparatus, including the optic fiber scanners, was immersed in a water bath thermostated to $\pm 0.05^{\circ}C$. Temperature

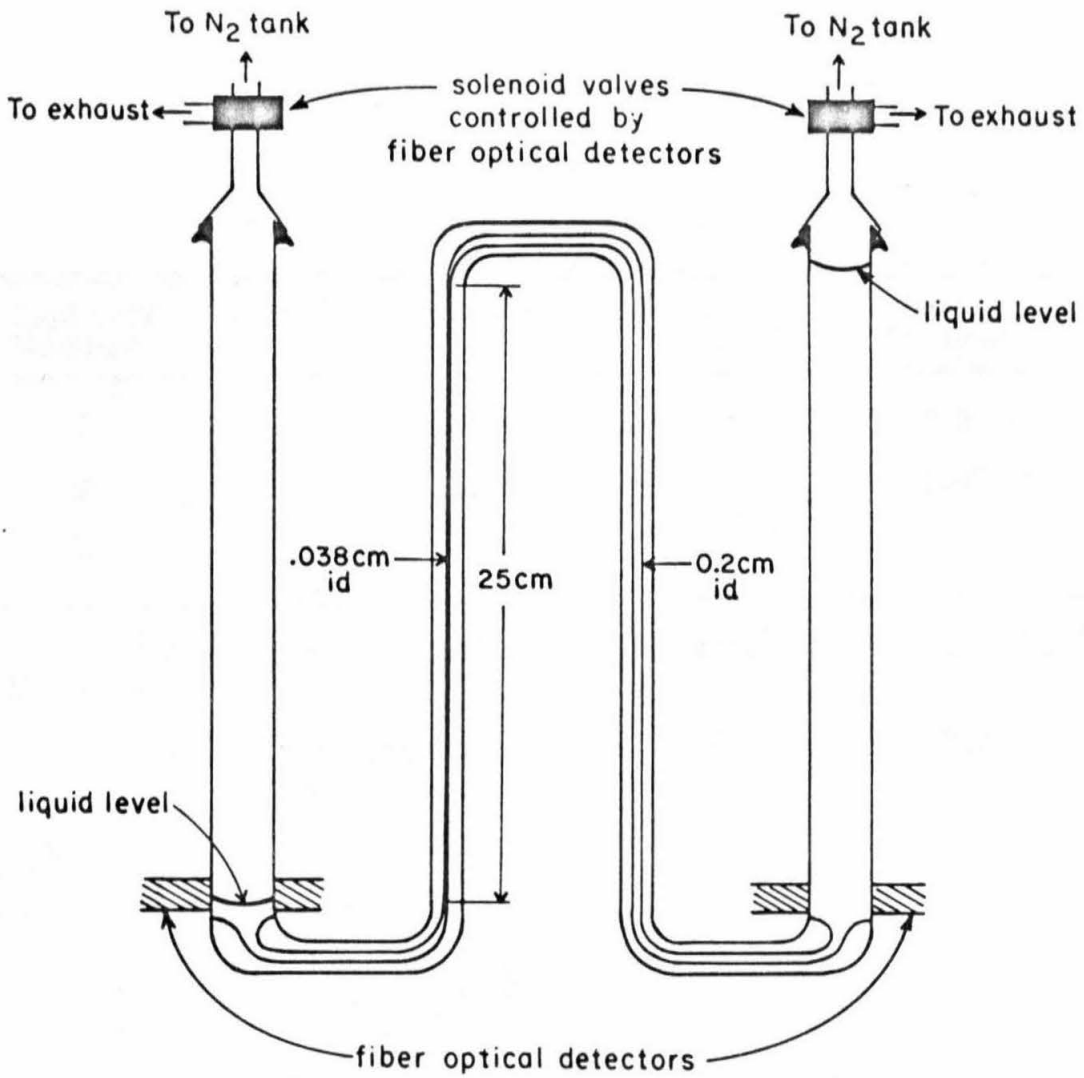

Fig. 1. Schematic drawing of a 25 cm. capillary (capillary #1 in Table I). Note that the liquid level in the left-hand reservoir is the lowest level reached by the liquid. At the position shown, the meniscus intersects the light beam between the fiber optical detectors (called optic fiber scanners or light pipes in the text). The volume of solution between this liquid level and the capillary and the corresponding volume between the capillary and the right-hand light pipes make up the dead volume referred to in the Experimental section and Table I.

Table I

Capillary Dimensions

Capillary Number	Length (cm)	Diameter (cm)	Reservoir Vol (ml)	Dead Vol (ml)	Max Psi †
1	24.5	0.0383	10	2.4	38
2	25.3	0.0383	15	1.4*	46
3	90.0	0.04	35	3.1	160

†Max Psi = nitrogen pressure in lb/in^2 at which Re = 2200 for H_2O at 25°C.

*In dichroism experiments the dead volume is 2.2 ml.

was measured by a thermometer standardized with an NBS thermometer.

In the event a shear breakage apparatus of the type used here may be useful to others, complete specifications are given in Appendix A.

Basic Fluid Mechanical Considerations

For laminar flow in a capillary, the liquid velocity is zero at the capillary wall and maximal in the center. When end effects can be neglected, the velocity at a distance r from the center of the capillary is

$$v(r) = \frac{P}{4L\eta}(a^2 - r^2) \qquad (1)$$

where v(r) is the liquid velocity in centimeters per second; P is the pressure differential between entrance and exit of the capillary in dynes per square centimeter; L is the capillary length in centimeters; η is the solution viscosity in poise and a is the capillary radius in centimeters.

Integrating the volume element $v(r)2\pi r\,dr$ over all r, we obtain Poiseulle's Law,

$$V = \frac{P\pi}{2L\eta}\int_0^a (a^2 - r^2)r\,dr = \frac{P\pi a^4}{8\eta L} \qquad (2)$$

where V is the volume flow rate in cubic centimeters per second.

The shear gradient is defined by

$$G \equiv -\frac{dv(r)}{dr} \tag{3}$$

It has units of reciprocal seconds and may be expressed in terms of the pressure differential, P, or volume flow rate, V.

$$G = \frac{Pr}{2L\eta} = \frac{4Vr}{\pi a^4} \tag{4}$$

The shear gradient is a linear function of the distance from the capillary center. It is zero at the center and maximal at the capillary wall. The maximum shear gradient is

$$G_m = \frac{Pa}{2L\eta} = \frac{4V}{\pi a^3} \tag{5}$$

The maximum shear stress is

$$\eta G_m = \frac{Pa}{2L} = \frac{4V\eta}{\pi a^3} \tag{6}$$

This quantity has units of dynes per square centimeter. It is important because in all conventional theories, the breaking force on a rigid rod molecule is proportional to the shear stress.

The Reynolds' number for flow in a capillary is

$$Re = \frac{P\rho a^3}{4L\eta^2} = \frac{2\rho V}{\pi\eta a} \tag{7}$$

where ρ is the density of the solution. The usual condition for the transition from laminar to turbulent flow is $Re \geq 2200$. In practice

higher Reynolds' numbers may be achieved without turbulence if the entrance and exit of the capillary are smooth and tapered. No turbulent flow was evident in our capillaries up to a Reynolds' number of about 7000. However, in only one experiment reported here does the Reynolds' number exceed the traditional limit of 2200.

The solution just entering a capillary does not have the parabolic velocity distribution characteristic of steady state flow. A certain distance is required to approach the steady state. For a capillary of diameter 2a this distance has been estimated as 0.058a Re.[17]

Not all the energy required to push a solution through a capillary is used in overcoming viscous forces. Some energy is used in accelerating the liquid from zero velocity to flow velocity. This energy is not regained when the solution issues from the opposite end of the capillary. The equations above presuppose that this energy comprises a negligible fraction of the total. For the flow velocities encountered in this work, the supposition is false. Thus a correction, called the kinetic energy correction, must be applied. If P is the total pressure differential, then the pressure drop used in overcoming viscous forces, $P_{corr.}$, is

$$P_{corr.} = P - \frac{\rho V^2}{\pi^2 a^4} \quad . \tag{8}$$

It is this quantity which should be used in calculating shear stresses, etc. Note that if one uses volume flow rate data instead of pressure data, this correction is unnecessary.

Breakage Rate in a Capillary

In laminar flow, the shear gradient and residence time of a volume element of the liquid flowing through the capillary are a function of the radial position of that volume element. Due to the parabolic flow pattern, the largest gradients and longest residence times are near the wall and the lowest gradients and shortest residence times are close to the center. The breakage rate, being a function of both gradient and residence time, will vary as a function of radial position. The amount of breakage per pass observed in the solution is an average of the rate at each radius, weighted by the amount of material flowing through the capillary at that radius and the residence time for that radius.

From measurements of the average breakage rate as a function of G_m, a rate constant for a specific shear gradient can be calculated. We anticipate that the rate of breakage will be first order in the concentration of unbroken DNA. At a given shear gradient, G, the breakage rate is

$$-\frac{dc}{dt} = k(G)c \qquad (9)$$

where c is the concentration of unbroken molecules. As indicated, the rate constant for breakage is expected to be a function of the gradient, G. The time available for reaction is the residence time, t(r), of a DNA molecule flowing, in laminar flow, through the capillary at radius r with its associated shear gradient, G.

Therefore, after one pass,

$$c = c_0 e^{-k(G)t(r)} \tag{10}$$

where c_0 is the initial concentration of whole molecules.

The probability of breakage per pass at the given G is then

$$P(G) = \frac{c_0 - c}{c_0} = 1 - e^{-k(G)t(r)} \tag{11}$$

The amount of DNA broken per unit time at the given radius is the probability of breakage per pass times the amount of DNA flowing through the capillary at this radius per unit time, $2\pi r\,dr\,v(r)c_0$. Therefore, the total amount broken per unit time is

$$2\pi c_0 \int_0^a v(r)P(G)r\,dr \tag{12}$$

The time for all the solution to pass through the capillary is φ/V where φ is the total solution volume. The amount of DNA broken per pass is $\varphi(c_0 - c)$ and

$$\varphi(c_0 - c) = \frac{2\pi c_0 \varphi}{V} \int_0^a v(r)P(G)r\,dr \tag{13}$$

But since the average probability of breakage per pass $\langle P \rangle$, is $(c_0 - c)/c_0$,

$$\langle P \rangle = \frac{2\pi}{V} \int_0^a v(r)P(G)r\,dr \tag{14}$$

This expression may be simplified using (1) and (2):

$$\langle P \rangle = \frac{4}{a^2} \int_0^a \left(1 - \frac{r^2}{a^2}\right) P(G) r \, dr \tag{15}$$

It will be convenient to change the integration variable from r to G. From (4) and (5),

$$G = G_m \left(\frac{r}{a}\right); \qquad r = a\left(\frac{G}{G_m}\right); \qquad dr = \left(\frac{a}{G_m}\right) dG \tag{16}$$

Equation (15) becomes

$$\langle P \rangle = \frac{4}{G_m^2} \int_0^{G_m} \left(1 - \frac{G^2}{G_m^2}\right) P(G) G \, dG \tag{17}$$

This integral cannot be evaluated because P(G) is some unkown function of G. However, we can use Equation (17) to calculate the rate constant, k(G). For the present, we will assume P(G) is much less than unity. This allows us to rewrite Eq. (11) as follows;

$$P(G) = 1 - e^{-k(G)t(r)} \approx 1 - 1 + k(G)t(r) = k(G)t(r) \tag{18}$$

Substituting in Eq. (17) and noting that $t(r) = L/v(r)$ where L is the capillary length,

$$\langle P \rangle = \frac{8L}{aG_m^3} \int_0^{G_m} \left(1 - \frac{G^2}{G_m^2}\right) \frac{k(G)G}{(1 - G^2/G_m^2)} \, dG \tag{19}$$

or

$$\langle P \rangle = \frac{8L}{aG_m^3} \int_0^{G_m} k(G)G \, dG \tag{20}$$

Differentiating the product $\langle P \rangle G_m^3$ with respect to G_m we obtain,

$$\frac{d(\langle P \rangle G_m^3)}{dG_m} = 3\langle P \rangle G_m^2 + G_m^3 \frac{d\langle P \rangle}{dG_m} \tag{21}$$

and from (20)

$$\frac{d(\langle P \rangle G_m^3)}{dG_m} = \frac{8L}{aG_m^3} k(G_m)G_m \tag{22}$$

Equating (21) and (22) we arrive at an expression for $k(G_m)$.

$$k(G_m) = \left(\frac{a}{8L}\right) \langle P \rangle Gm \left[3 + \frac{d \ell n \langle P \rangle}{d \ell n G_m}\right] \tag{23}$$

All the quantities on the right are experimentally accessible. Equation (23) gives us the breakage rate constant at G_m from measurements of the average breakage probability as a function of G_m. Its validity is dependent on the assumption that $k(G)t(r) \ll 1$. Clearly this condition fails in any experiment near the capillary wall where the residence time, $t(r)$, is extremely long. An analysis of the problem indicates that if $\langle P \rangle \leq 5 \times 10^{-3}$, a negligible fraction (10%) of the total breakage occurs in a region where the assumption $k(G)t(r) \ll 1$ fails (see Discussion); therefore, if $\langle P \rangle \leq 5 \times 10^{-3}$, Eq. (23) may be used to calculate $k(G_m)$.

The design of the capillary devices is such that not all of the liquid passes through the capillary on each pass (see Figure 1). The residual volume, called the dead volume, V_d, is mixed with the sheared solution upon its return to the reservoir. The measured concentration of halves and the observed breakage probability are lower than they would be if all the solution passed through the capillary. To obtain the true probability of breakage per pass, a correction must be applied.

Let V_t be the total solution volume and V_p the volume actually passing through the capillary. $V_t = V_p + V_d$. Let c_0 be the initial concentration of unbroken molecules, c be the concentration in the pass solution V_p after one pass, and c′ be the intact molecule concentration in the total mixed solution, V_t. At the end of the pass,

$$\langle P \rangle = \ell n \left(\frac{c_0}{c}\right) \tag{24}$$

$$c' V_t = c_0 V_d + c V_p$$

where $\langle P \rangle$ is the actual breakage probability. The observed probability, $\langle P \rangle'$ is

$$\langle P \rangle' = \ell n \frac{c_0}{c'} = \ell n \left[c_0 \Big/ \left(\frac{V_p}{V_t} c + \frac{V_d}{V_t} c_0 \right) \right] \tag{25}$$

This can be rearranged to

$$\langle P \rangle' + \ell n \left(\frac{V_p}{V_t} \right) = \ell n \frac{c_0}{c} \left(\frac{1}{1 + (V_d / V_p)\, e^{\langle P \rangle}} \right) \tag{26}$$

where $e^{\langle P \rangle} = c_0/c$. Using (24),

$$\langle P \rangle = \langle P \rangle' + \ell n\left(\frac{V_p}{V_t}\right) + \ell n\left(1 + \frac{V_d}{V_p}\, e^{\langle P \rangle}\right) \tag{27}$$

Introducing series expansions for $e^{\langle P \rangle}$ and $\ell n(1 \pm x)$

$$\langle P \rangle \approx \langle P \rangle' - \frac{V_d}{V_t} - \tfrac{1}{2}\left(\frac{V_d}{V_t}\right)^2 + \frac{V_d}{V_p} + \langle P \rangle \frac{V_d}{V_p} - \tfrac{1}{2}\left(\frac{V_d}{V_p}\right)^2 (1+p)^2 \tag{28}$$

We can eliminate V_p using the relation $V_p = V_t - V_d$.

$$\langle P \rangle \approx \langle P \rangle' - \frac{V_d}{V_t} - \tfrac{1}{2}\left(\frac{V_d}{V_t}\right)^2 + \frac{V_d}{V_t(1 - V_d/V_t)} + \langle P \rangle \frac{V_d}{V_t(1 - V_d/V_t)} - \tfrac{1}{2}\left(\frac{V_d}{V_t(1 - V_d/V_t)}\right)^2 (1 + 2\langle P \rangle + \langle P \rangle^2) \tag{29}$$

Each of the terms containing $(1 - V_d/V_t)^{-1}$ may be expanded according to the series

$$\text{for } x^2 < 1, \quad (1-x)^{-n} = 1 + xn + \frac{n(n+1)}{2!}\, x^2 + \ldots$$

Taking only the first two terms in each expansion and neglection $\langle P \rangle^2$ and $(V_d/V_t)^3$ terms we arrive at the simple relation

$$\langle P \rangle \approx \langle P \rangle' + \langle P \rangle \frac{V_d}{V_t}$$

or

$$\langle P \rangle \approx \langle P \rangle' \Big/ \left(1 - \frac{V_d}{V_t}\right) \tag{30}$$

The correction factor $(1 - V_d/V_t)^{-1}$ was typically 1.2 for the 25 cm capillary (# 2) and 1.4 for the 90 cm capillary. Over the duration of an experiment, V_t changes since samples are withdrawn periodically. However, the samples are sufficiently small so that the correction factor only changes by $\leq 3\%$.

DNA Preparation

DNA from the mutant bacteriophage $\lambda b_2 b_5 c$, molecular weight 25×10^6 daltons, was used exclusively in this work. Stocks were obtained from those maintained by Dr. J. J. Weigle and Dr. J. S. Parkinson. Phage were produced by innoculating a liter culture of E. coli K12 W3110 (concentration 2×10^8 cells/ml) with enough phage to infect every 20^{th} bacterium. The culture was allowed to grow for two generations of phage. Yields of $1\text{-}3 \times 10^{11}$ phage particles per milliliter were routinely achieved. A complete description of the procedure is given in the form of a recipe in Appendix B.

The DNA was extracted following the phenol technique of Mandell and Hershey.[18] For convenience this is also given in Appendix B. The DNA was dialyzed twice against 0.1 F Na_2EDTA adjusted to pH 8 with NaOH. It was then dialysed four or five times against 0.075 F NaCl, 0.01 F Na_2EDTA and 0.005 F phosphate pH 7.0. The concentration of NaCl given is approximate. The solution was made up to be

exactly 0.1 F in sodium ion to which the Na_2EDTA, sodium phosphate (and the NaOH used to adjust the pH) contribute. The DNA was stored over chloroform at 4°C.

When long storage periods were necessary, the DNA was kept as phage. No increase in random single strand breaks were observed by alkaline sedimentation as a result of storing phage (over chloroform) for as long as five months. Every three months or so an aliquot of phage was phenol extracted and dialyzed. It had an $A_{260}^{1\,cm}$ between one and two. It remained at this concentration, over chloroform, until it was used. $S_{20,w}$ for this DNA at pH 7 was 31.5 ± 0.8S.

The number of single strand breaks present in the DNA was determined by two methods. The first of these was band sedimentation. About 30% of the DNA trailed behind the main band in a band velocity sedimentation performed under denaturing conditions (Figure 3). This corresponds to about 0.3 breaks per single strand.

The second estimation of the number of single strand breaks per molecule was accomplished with the help of Dr. Martha Simon. She denatured some DNA with alkali and renatured it in the presence of 40% formamide. After removing the formamide by dialysis, she mounted the DNA on an electron microscope grid using the Kleinschmidt basic film technique.[19] A histogram of the resulting DNA as viewed in the electron microscope is shown in Figure 2(a). Molecules with no attached single strand regions and those showing single strand regions at one or both ends were scored. One half the molecules traced out of a total population of 156 were shorter than whole unbroken $\lambda b_2 b_5 c$ DNA.

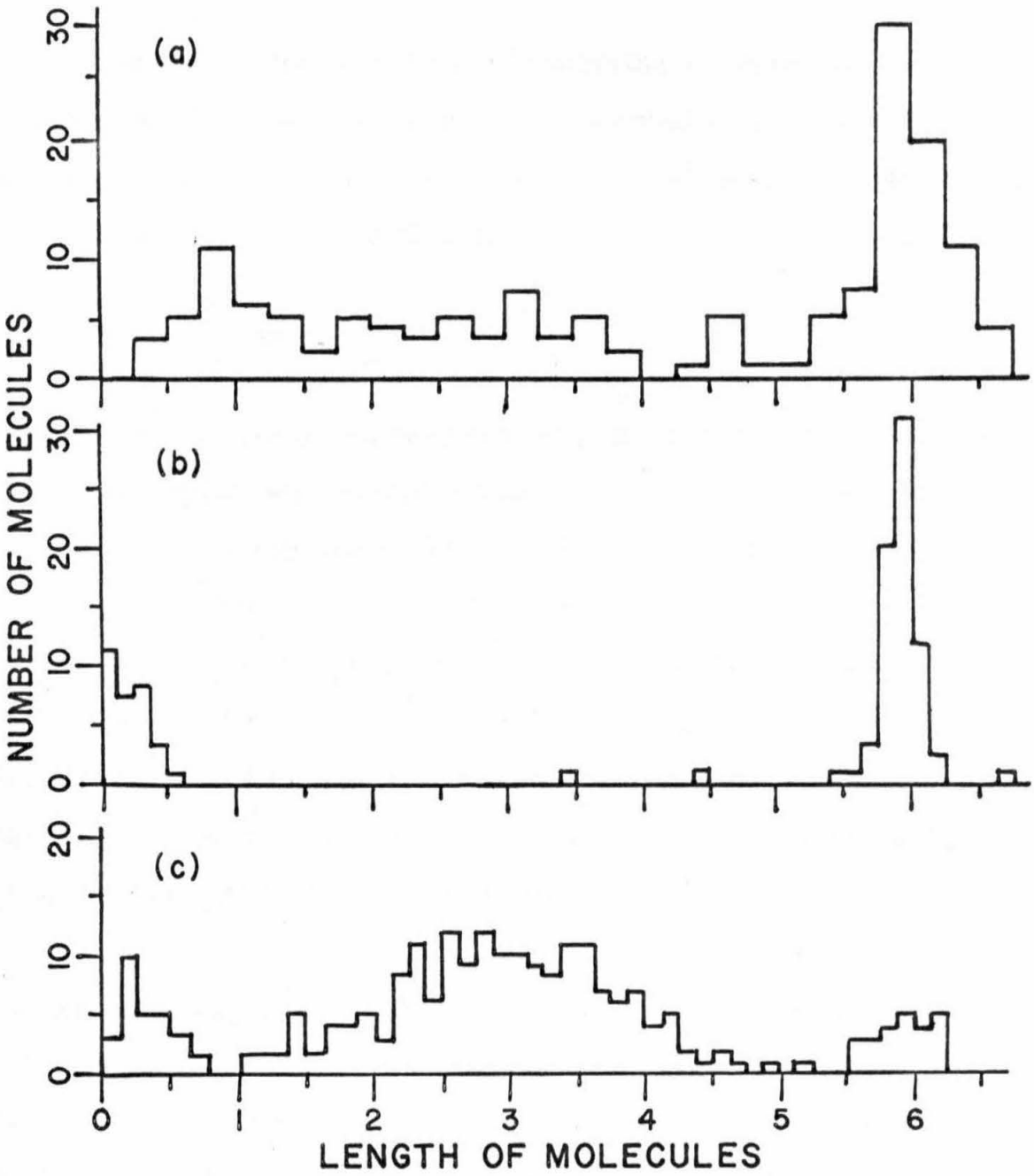

Fig. 2. Histograms of $\lambda b_2 b_5 c$ DNA. (a) DNA which was denatured in alkali, neutralized and renatured in the presence of formamide (see text); (b) native whole molecules; (c) native half and whole molecules. The half molecules were prepared by passing the 7.5 μg/ml DNA solution shown in (b) through capillary #3 (Table I) 2100 times at 131 psi and 25°C. The units on the abcissa are proportional to the length of the DNA molecules as they appear in electronmicrographs.

Let P(x) be the probability of observing x breaks in a single stranded DNA. If the number of breaks is small compared to the number of intact bonds (which the centrifuge data indicate), the probability P(x) will be a Poission distribution

$$P(x) = \frac{\mu^x e^{-\mu}}{x!} \qquad x = 0, 1, 2, \ldots \tag{31}$$

where μ is the average number of breaks per strand. The probability of finding a double stranded DNA with no single strand breaks is P(0)P(0). The probability of finding x_1 breaks in one strand and x_2 breaks in the other strand of a double stranded DNA is $2P(x_1)P(x_2)$.

From these relations, it is easy to show that in a population of native DNA with $\mu \approx 0.3$, the probability of finding a molecule with two or more breaks in one of its strands is very small. We shall neglect these molecules. Thus we expect a reasonable representation of the denaturation and subsequent renaturation to be:

In this diagram as well as in the discussion which follows, we have assumed that short pieces of DNA which arise from single strand breaks always renature with a whole sized single strand. The renatured, double stranded molecules are then of two types, whole unbroken molecules which have the appearance of native $\lambda b_2 b_5 c$ DNA and molecules which are shorter than the native DNA length. The letters in

front of each molecular species stand for the number of molecules of that type.

There are specific relations between the number of each type of molecule present in the original population. The ratio of un-nicked molecules to one-nicked molecules is

$$\frac{n}{m} = \frac{P(0)P(0)}{2P(1)P(0)} = \frac{e^{-2\mu}}{2(\mu e^{-2\mu})} = \frac{1}{2\mu} \tag{32}$$

The ratio of one-nicked molecules to two-nicked molecules is

$$\frac{m}{r} = \frac{2P(1)P(0)}{2P(1)P(1)} = \frac{2(\mu e^{-2\mu})}{2(\mu e^{-\mu})^2} = \frac{1}{\mu} \tag{33}$$

If we assume that all the short single strand molecules re-nature, the following equations apply.

$$\begin{aligned} v &= 2m + 4r \\ s &= \frac{2n + m - v}{2} \end{aligned} \tag{34}$$

We observe in the microscope that there are equal numbers of s and v type molecules so that

$$n = \frac{5m + 12r}{2} \tag{35}$$

The fraction of single strands in the original DNA preparation which have a break is

$$\mu = \frac{m + 2r}{2n + 2m + 2r} \tag{36}$$

From Eqs. (32), (33), (35) and (36) we can solve for μ, the average number of breaks per single strand. Under the assumption that all the short single strand pieces renature, μ is 0.14 breaks/strand. Similarly, if we assume only one half of the short pieces renature, we arrive at

$$v = m + 2r \tag{37}$$

and we find that in this case, $\mu = 0.25$. We conclude from the foregoing analysis that a good estimate for the number of breaks per single strand in the original DNA preparation is about 0.25.

Breakage Experimental Procedure

Normal experimental procedure begins with dilution of stock DNA with buffer (0.1 F total Na^+, 0.01 F EDTA, 0.005 F phosphate, pH 7.0) to the desired concentration, typically 7.5 μg/ml. The total solution volume was usually 10 ml. A UV spectra of the diluted DNA was recorded with a Cary 14 Spectrophometer after which the DNA solution was gravity filtered through a Millipore filter, pore size 8μ. The effluent from the filter was fed directly into a reservoir of the capillary apparatus through Teflon tubing. The Millipore filter support was Kel-F. At no time did the DNA solution come in contact with metal surfaces (except in experiments using flow dichroism).

Before shearing the DNA it was necessary to break apart any paired "sticky ends" of the λ molecules which had caused formation

of circles and dimers. In early experiments this was done prior to filtering by heating the DNA at 75°C for five minutes (in buffer containing 0.1 F Na^+) and quenching in ice. This procedure introduced many single strand breaks and it was abandoned in favor of separating paired sticky ends with shear stress.

Hershey circles, the major contaminant, were converted to linear monomers in 200 passes through a 25 cm long capillary at a maximum shear stress of 630 dynes/cm^2 (25°C, DNA concentration 7.5 μg/ml). This treatment caused less than 1% of the linears to break into half molecules (as estimated using Table II below).

After a control sample of 100% linears was withdrawn, breakage of the linear molecules began at a higher nitrogen pressure. The volume flow rate was obtained from measuring the pass time for 5 ml. Capillaries 2 and 3 have volume graduations for this purpose. The volume flow rate was accurate within 1%. At periodic intervals the flow was stopped, the pass number was recorded and a 0.15 ml sample was withdrawn. It was immediately transferred to a refrigerator at 4°C where it was kept until centrifugation. Normally, samples were analyzed within one or two days. No change in the percentage of whole molecules was evident after storage at 4°C for as long as a week. Thus the rate of forming end-to-end joined molecules during storage was negligible.

During the rest of the breakage experiment, passage times were recorded and the volume flow rate was periodically checked. These two data give the correction to the breakage probability required by the dead

volume according to Eq. (30).

Sedimentation Analysis

Samples removed from the capillary apparatus were analyzed for percentages of intact and broken molecules by band velocity sedimentation in a Spinco Model E ultracentrifuge. For machines equipped with a monochromator and photoelectric scanner, 40 μl of DNA solution was layered on 3 M CsCl (density 1.37) in double sector, 30 mm, band forming center pieces (type II-modified). The CsCl was buffered at pH 7 with 0.0025 M phosphate and 0.005 M EDTA. To obtain flat base lines, 40 μl of buffer, containing an EDTA concentration equal to that of the DNA solution, was layered on the CsCl solution in the reference sector.

For machines equipped with a mercury lamp and photographic plates, 70 μl of DNA solution was layered on 3 M CsCl in a single sector, 30 mm, band forming center piece (type III). Minus 2° radial wedges were required to compensate for the density gradient generated during a run. The rotor was spun at around 31,000 rpm at about 22°C. Films were traced with a Joyce-Loebl microdensitometer. For alkaline sedimentations, the 3 M CsCl was also 0.1 M in NaOH.

Typical sedimentation profiles are shown in Figure 3. The DNA peaks in each scan were traced, cut out and weighed. The weight fraction of whole molecules was determined from the ratio of the wholes peak area to the halves peak area of each scan. The error introduced due to the sector shape of the centrifuge cell was less than 4% and was

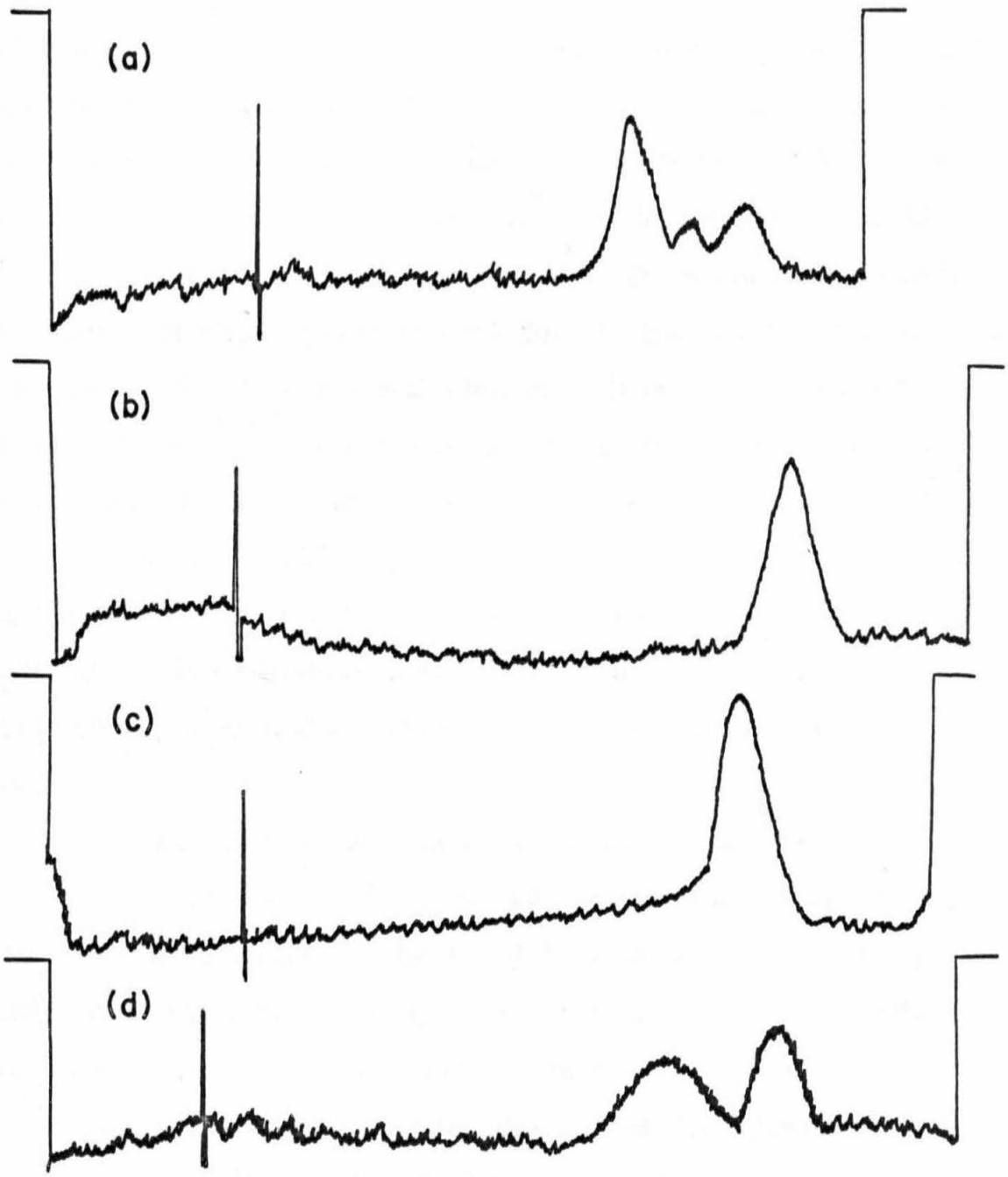

Fig. 3. Typical band sedimentation profiles of $\lambda b_2 b_5 c$ DNA in 3M CsCl. The direction of sedimentation is left to right. (a) native phenol extracted phage DNA showing monomer, monomer circle and dimer peaks; (b) native linear molecules; (c) denatured linear molecules; (d) native half and whole linear molecules. See text for sedimentation conditions.

ignored. The standard deviation of the weight fraction of whole molecules for a single sample during one centrifuge run was typically 0.05. For this reason, the fraction of whole molecules was always determined from the average of as many scans of the sample as possible. Normally four to seven scans were taken. The standard deviation of the fraction of whole molecules for a sample in several centrifuge runs was about 0.05. A sample was analyzed only once except when a large deviation (≥ 0.15) was suspected. When less than 15% of either component was present, it was impossible to obtain reliable percentages.

A solution of 50% whole molecules obtained by mixing equal quantities of solutions containing 100% whole and 100% half molecules respectively was measured to have 47% whole molecules. Thus we consider this method of analysis accurate in measuring the extent of breakage.

The majority of experiments were performed with a DNA concentration of 7.5 μg/ml. Samples containing less than this amount of DNA had to be concentrated for the DNA bands to be visible in the centrifuge. The sample solutions were concentrated by evaporation under negative pressure at room temperature.

An apparatus was constructed which could evaporate 10 samples simultaneously. It consisted of 10 removable sample vials arrayed along a long glass conduit which in turn was connected to a vacuum pump through a dry-ice methanol trap. The evaporation rate was adjusted to keep the samples just above the freezing point, a procedure which was superior to lyophilization because of the difficulty in

redissolving concentrated DNA and salt. Sample volumes were chosen so that the concentrated solutions would contain 15 μg of DNA per ml. However, sedimentation scans of these concentrated solutions were similar to those containing 7.5 μg of DNA per ml.

It was observed that the evaporation procedure did not affect the percentage of broken molecules in a solution of 50% halves.

Flow Dichroism Analysis

The flow dichroism apparatus built by Callis and Davidson[24] offered a quick, easy method for measuring the amount of breakage. A dichroism measurement takes less than one-fourth the time of a centrifuge run and can be used to monitor breakage as it occurs. When using sedimentation analysis, the results of an experiment could be learned only after its completion. (Except for very long experiments, it was impractical to operate the breakage apparatus and a centrifuge simultaneously.) Too often the major finding was that no breakage occurred or that it occurred too quickly.

Capillary 2 (Table I) has provision for connecting the dichroism cell in parallel with the capillary. To make a flow dichroism measurement, the nitrogen gas pressure was reduced to about 9 pounds per square inch. The pressure was constant for all dichroism measurements of any particular experiment. Appropriate (Teflon) stopcocks were opened to allow DNA to flow through the cell; shutting a stopcock stopped the flow. The difference in absorbence between the flowing and stationary states was recorded.

Flow dichroism is the quantity $\Delta A/A$ where ΔA is the absorbence difference between flowing and stationary states in the dichroism cell and A is the absolute absorbence of the stationary solution. Assuming a linear relationship between weight average molecular weight and dichroism for the molecular weight range 12.5 to 25 million, the amount of breakage was measured by interpolation between the dichroism values for solutions containing 100% whole and 100% half molecules, respectively. These dichroism values were obtained at the beginning and end of each breakage experiment.

Having the dichroism cell connected in parallel with the capillary introduced a dead volume which is not mixed with the sheared solution after a pass. To overcome this problem, every fifth pass was allowed to pass through both the capillary and the dichroism cell under the nitrogen pressure at which the DNA was being broken. The dimensions of the cell, capillary and associated lead tubing were such that (theoretically) 3.5 times as much solution passed through the cell as passed through the capillary. A pass correction was applied to the measured breakage probability to compensate for this procedure.

The maximum shear stress generated in the dichroism cell under these conditions was 0.83 of that generated in the capillary. Because only one pass in five went through the cell, because the cell length is one-third the capillary length, and because $(d\,\ell n k)/d\eta G)$ is 1.9×10^{-2} cm^2/dyne (see Results), less than 0.5% of the breakage occurred in the dichroism cell. The control experiment comparing breakage rates with and without using dichroism was not done because

analysis by flow dichroism was abandoned. It was feared metal ions picked up from the titanium dichroism cell might influence the rate of breakage. Flow dichroism is not used in any experiment from which quantitative results are derived. However, flow dichroism was used in several experiments from which important qualitative inferences are drawn (see Figure 7).

RESULTS

Half-sized $\lambda b_2 b_5 c$ DNA molecules produced by shear breakage of linear monomer molecules had a sedimentation coefficient, $s_{20,w}$, of $24.6 \pm 0.8S$ corresponding to a mean molecular weight of 12.6×10^6 daltons.[20] A cursory comparison of whole and half molecule sedimentation bands (Figure 3) indicates the halves are less homogeneous in molecular weight than are the whole molecules. Histograms compiled from electronmicrographs of broken and unbroken $\lambda b_2 b_5 c$ DNA (Figures 2(b), (c)) confirm this conclusion.

The standard deviation in length of the whole DNA molecules (Figure 2(b)) is about 2% of their average length. This deviation probably arises from the procedures of mounting, photographing and measuring the length of the DNA rather than from any real distribution in length of the phage DNA. The half molecule histogram (Figure 2(c)) is normally distributed and is much broader than the whole molecule histogram. The standard deviation in length for half molecules is 27% of their average length. Allowing 2% to measurement error, the remaining 25% represents the standard deviation in the point of breakage. In terms of the unbroken molecular length, the standard deviation in the breakage point is 12.5% or $1.6\ \mu$ from the center of the molecule. Since the breaks appear normally distributed, we can say that two-thirds of the breakage occurs in the central quarter of the $\lambda b_2 b_5 c$ DNA molecule.

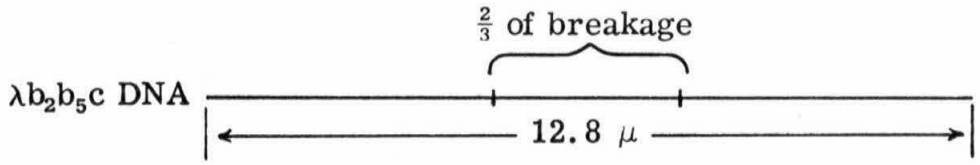

Somewhat similar results were obtained from careful analysis of a sedimentation band of half molecules. The method[21] is less accurate than electron microscopy when it is applied to the dilute DNA bands encountered in this work. The tails of the distribution in Figure 2(c) are hidden in the noise of the centrifuge's scanning system and the molecular weight distribution appears more narrow than it probably actually is. However, within the limits imposed by the scanner noise level, the two methods give identical results (see Appendix D).

The shear stress required to break DNA at a given rate increases with increasing DNA concentration. This phenomenon has been called the self-protection effect. The shear stress required to produce at least a detectable amount of breakage (about 15 weight-% halves) in 100 passes (25 cm long capillaries) is plotted in Figure 4 as a function of DNA concentration over the range 0.05 μg/ml to 7.5 μg/ml. The line shown in the figure has a slope of 23 dynes/cm^2 per μg/ml.

In the rest of the breakage experiments, it was convenient to use 7.5 μg DNA/ml. At this concentration, 40 μl samples taken from the breakage apparatus and put directly into the centrifuge cells produced fairly large well defined peaks. The self-protection effect is quite evident at this concentration as Figure 4 shows. Extrapolation of the line in the figure to zero DNA concentration yields a shear stress

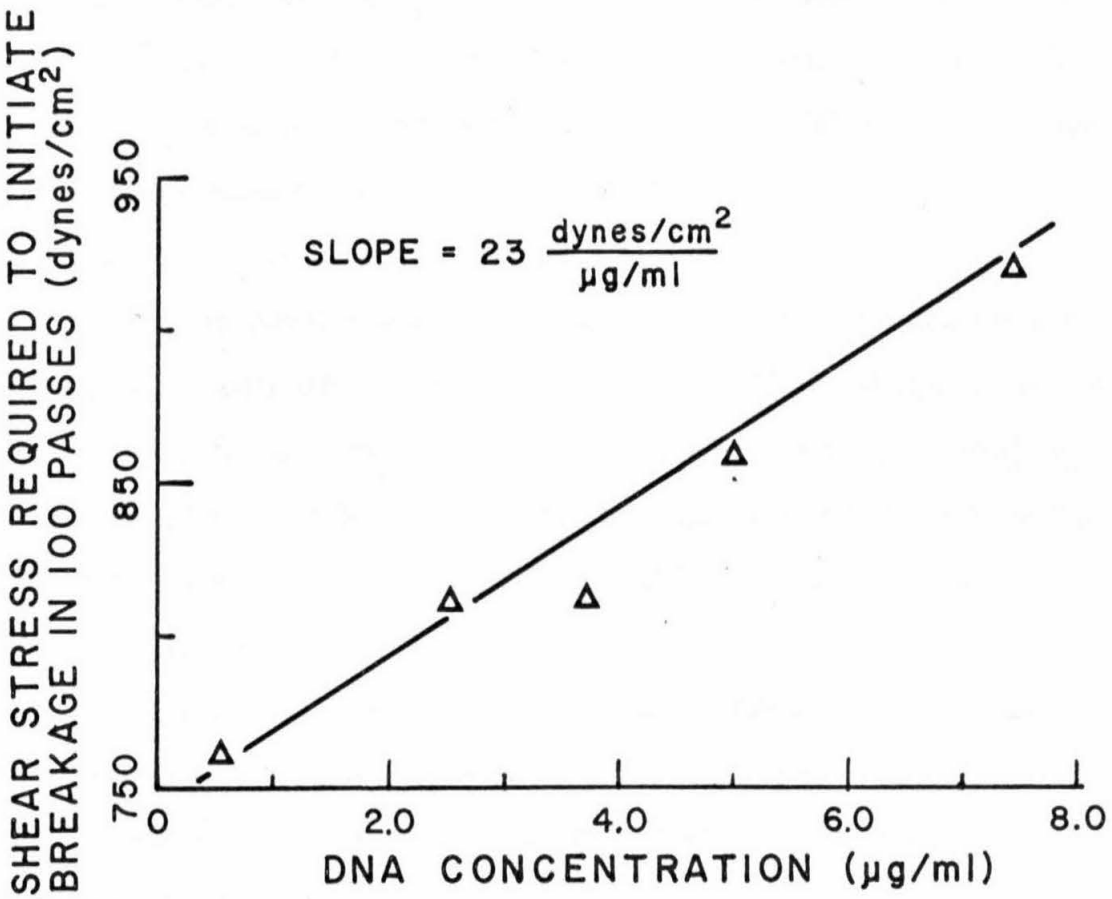

Fig. 4. This figure demonstrates the self-protection effect. It shows that the shear stress (at the capillary wall) required to initiate breakage in 100 passes through capillary #1 or #2 (Table I) increases with increasing DNA concentration. These experiments were conducted at 25°C in a buffer consisting of 0.01 F Na_2EDTA and 0.005 F Na_2HPO_4 adjusted to pH 7.0 with NaOH and with enough NaCl added to bring the total sodium ion concentration to 0.1 F.

substantially lower than that required to initiate breakage in a 7.5 μg DNA/ml solution. We will assume that self-protection is not a function of temperature, viscosity and salt concentration, and that measuring the effects of these and other variables with 7.5 μg DNA/ml solutions gives the same results as would be obtained by extrapolating each measurement to zero DNA concentration.

The concentration range of Figure 4 probably includes the lower concentrations normally required in everyday DNA handling. To assist those who wish to take precautions against shear breakage, the flow rate required to generate a shear gradient sufficient to break $\lambda b_2 b_5 c$ DNA (molecular weight 25×10^6 daltons) is plotted against capillary diameter in Figure 5.

Some very preliminary experiments concerned with preparing quarter sized λ molecules indicated that the flow rate required to break DNA is inversely proportional to the first power of molecular weight. The reader is reminded of the theoretical treatment of shear breakage by Levinthal and Davison[4] which predicts the "critical flow rate" should change with the second power of molecular weight.

According to results presented below, temperature does not influence the magnitude of the "critical flow rate". It should be born in mind that Figure 5 was calculated from experiments performed with a capillary having a smooth, tapered entrance and exit. Turbulence may be generated at the abrupt end of the pipet, for example, which would tend to increase the likelyhood of breakage.

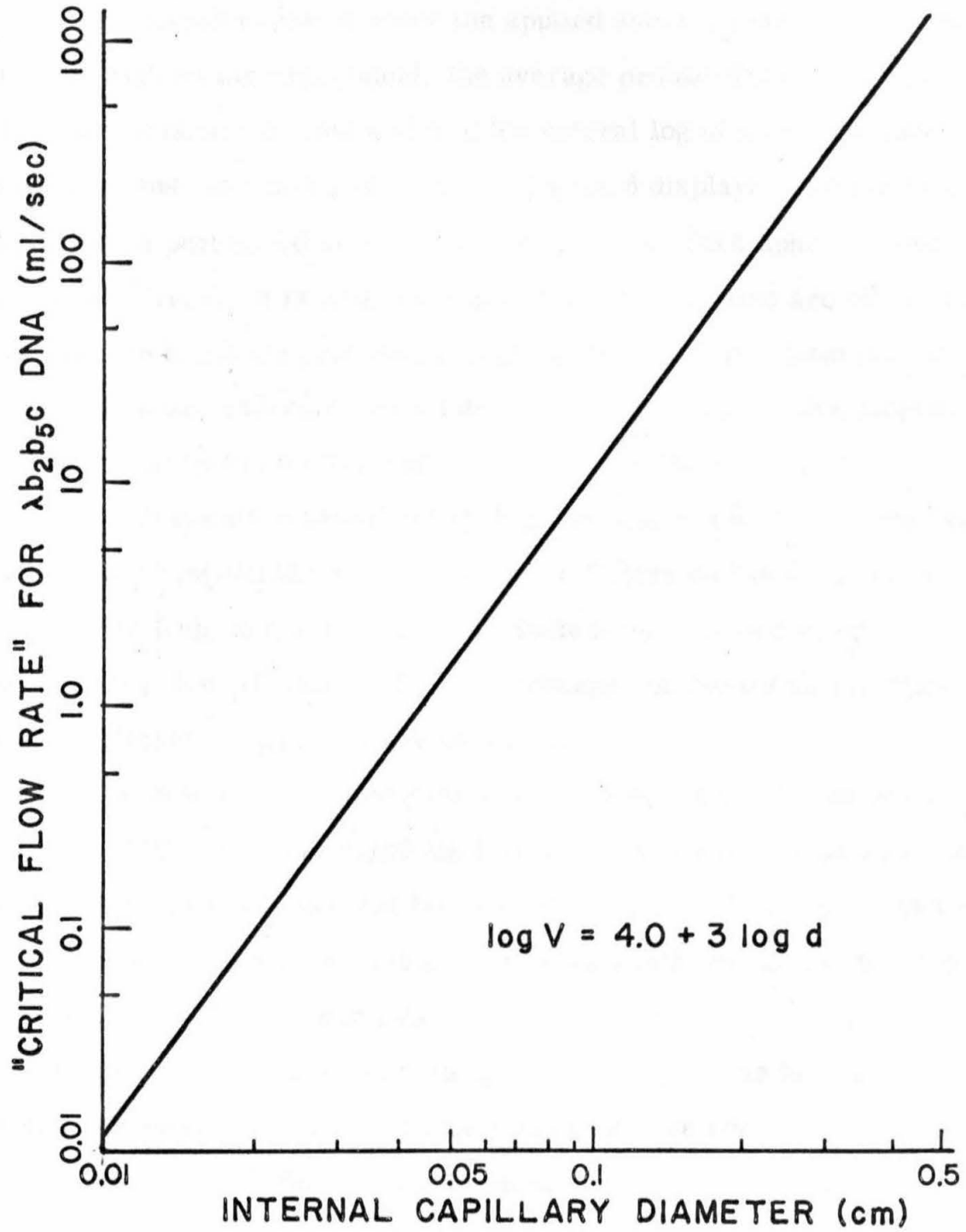

Fig. 5. The flow rate required to produce a shear stress sufficient to break $\lambda b_2 b_5 c$ DNA is plotted against capillary diameter. In the equation, V = flow rate (ml/sec) and d = internal capillary diameter (cm).

For experiments in which the applied shear stress remains constant throughout the experiment, the average probability of breakage, $\langle P \rangle$, may be obtained from a plot of the natural log of monomer concentration versus the number of passes. Figure 6 displays plots for three experiments performed at the same temperature, DNA concentration and shear stress. It is apparent that first order kinetics are followed. The average breakage probability is given in each case. Intervals of error shown are 95% confidence intervals for the straight line slopes. The dead volume correction has been applied to these numbers.

Experiments represented by Figures 6(a) and 6(b) differ only in their buffer concentrations. The buffer in Figure 6(b) is 6.25 times more dilute than that of Figure 6(a). Sodium ion concentrations are respectively 0.016 F and 0.1 F. The breakage probabilities for these two experiments are practically identical.

The reason for studying the effect of ionic strength was to test the hypothesis that shear breakage involves local denaturation under the influence of the stretching and bending caused by the flow field. As we shall see, there is a large temperature coefficient for breakage which is consistent with the denaturation hypothesis. Since Tm for denaturation decreases with decreasing ionic strength, the breakage rate should accordingly increase. Since it does not, we conclude that local denaturation is not important for breakage.

Figures 6(b) and 6(c) differ in the procedure by which the DNA solutions were prepared for breakage. Concentrated $\lambda b_2 b_5 c$ DNA stock solutions, from which material for breakage experiments is taken,

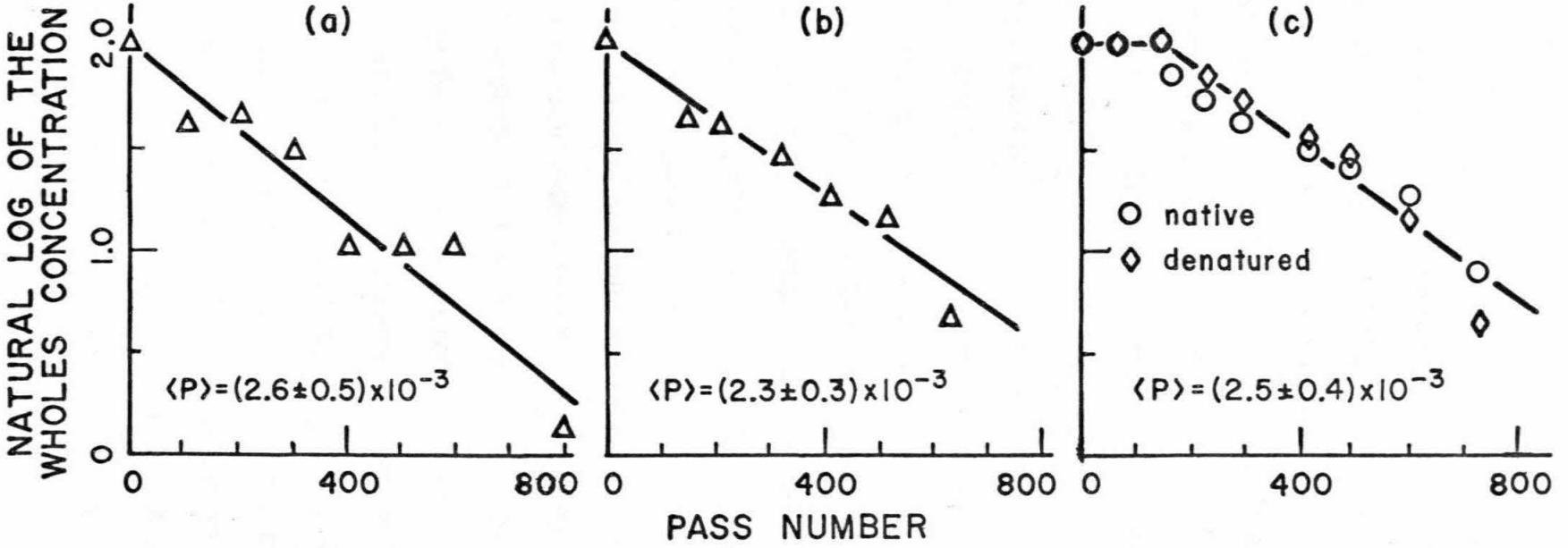

Fig. 6. The three experiments shown in this figure were performed at the same DNA concentration, temperature and shear stress using capillary #2 (Table 1). ([DNA] = 7.5 μg/ml, T = 25°C, ηG_m = 920 dynes/cm^2). The probabilities of breakage per pass, $\langle P \rangle$, correspond for the three experiments within experimental error. Experiments (a) and (b) differed in buffer concentration: (a)'s buffer was 0.01 F Na_2EDTA, 0.005 F Na_2HPO_4 adjusted to pH 7.0 with NaOH and with enough NaCl added to bring the total sodium ion concentration to 0.1 F. (b)'s buffer was (a)'s buffer diluted by a factor of 6.25. Experiments (b) and (c) differed in the procedure by which the DNA was prepared for breakage. See text for details. Note the fraction of whole molecules measured under denaturing conditions in (c) agrees with measurements on the native DNA.

consists of about 70% monomers and 30% Hershey circles and dimers. In Figure 6(b) (and Figure 6(a)), these hydrogen bonded forms are converted to linear monomers prior to breakage by passing the solution through the capillary at a shear stress which parts the hydrogen bonds but does not cause significant breakage of monomers. In Figure 6(c), the circles and dimers are not removed prior to breakage. The breakage probabilities for these two experiments, calculated from the straight lines shown in the figure, are the same within experimental error. There is a "lag period" at the beginning of the experiment of Figure 6(c) in which the breakage probability steadily increases to the final maximum value. This lag period is observed by other workers[3,22] and in other experiments in this thesis. Some of these experiments are plotted in Figure 7 which will be discussed immediately below. At the present it is important to notice from Figure 6(c) that the lag period shows up in band sedimentation under denaturing conditions and in band sedimentation under non-denaturing conditions. The weight percentage of half molecules at each point during the experiment is the same whether the DNA is denatured or native.

The three experiments of Figure 6 can be used to estimate the reproducibility of measuring $\langle P \rangle$. They differ somewhat in salt concentration and pre-breakage treatment, but these have been shown to have no effect on $\langle P \rangle$ at least over the ranges reported. The average of the three breakage probabilities is $(2.48 \pm 0.24) \times 10^{-3}$ where again the error interval is the 95% confidence interval. It indicates that breakage probabilities are reproducible within about 10%. However,

the average 95% confidence level for ⟨P⟩ of all experiments of this type is 0.16 ⟨P⟩. We conclude that ⟨P⟩ measurements are reproducible within about 15%.

We know about 12% of a typical DNA preparation has single strand breaks in the central quarter of the molecule. We therefore might expect in any experiment that these molecules would be broken first and we should observe a faster initial breakage rate. In Figures 6(a) and 6(b), as well as in all experiments of this type, the breakage rate appeared constant throughout. Using the band velocity sedimentation technique, one could not accurately measure less than about 15% half molecules by weight. Thus if the first 12% of the DNA did break faster than the rest, it is doubtful it would be detected. Within experimental error, the straight lines fitted to the points in plots such as those of Figures 6(a) and 6(b) extrapolate to 100% whole molecules at time zero.

Figure 7 shows three experiments which exhibit the lag phenomenon. They were performed prior to the observation that breaking Hershey circles by heating (75°C for 5 minutes in 0.1 F NaCl, 0.1 F EDTA, 0.005 F phosphate, pH 7) introduced many single strand breaks.[23] DNA used in these experiments was heat treated before breakage. Band velocity sedimentation showed no circles and dimers remained after this treatment. Thus the only difference between the experiments which exhibit lag periods (Figure 7) and those which do not (Figures 6(a), 6(b)) is the method by which hydrogen bonded circles and dimers are converted to monomers prior to breakage. Possible causes of this

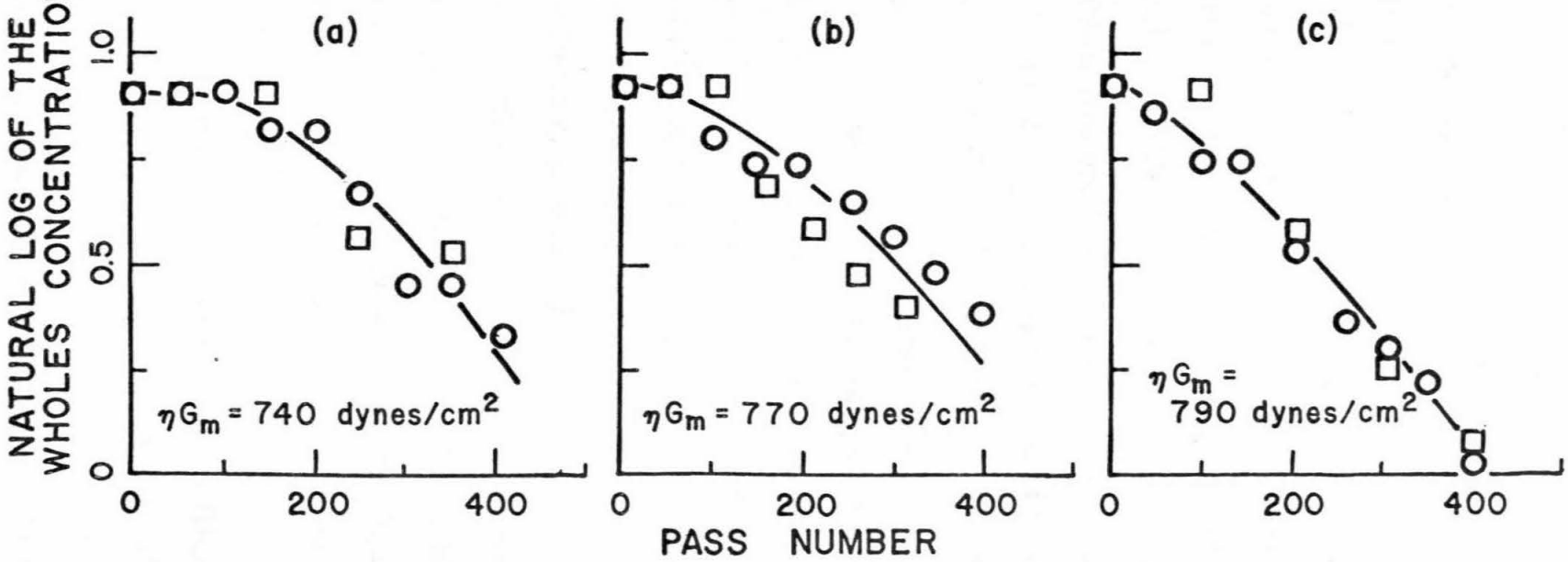

Fig. 7. These three experiments demonstrate the lag period phenomenon. The breakage rate at the beginning of each experiment lags behind the eventual steady state rate. Note the good agreement of the points obtained from flow dichroism (○) to those obtained from band sedimentation (□).

lag period will be considered in the Discussion. In the remainder of the experiments reported here, the lag problem was avoided by using shear stress, not heat, to convert all the DNA to the monomer form.

The experiments of Figure 7 are examples of those in which the extent of breakage was monitored by flow dichroism. One can see from the figure that this method gives data which agree well with the results obtained with band velocity sedimentation.

The dependence of breakage probability on shear stress at 10°C and 25°C is given in Table II and Figure 8. The breakage rate constants $k(G_m)$ are calculated with Equation (23) using the experimentally determined values for $(d \ell n \langle P \rangle)/(d \ell n G_m)$. It is evident that a small change in shear stress causes a large change in the breakage probability and $k(G_m)$. This is reflected in the magnitudes of $(d \ell n \langle P \rangle)/(d \ell n G_m)$ and $(d \ell n k)/(d\eta G_m)$. Note that $(d \ell n \langle P \rangle)/(d \ell n G_m)$ increases with decreasing temperature.

A preliminary experiment showed that a large temperature coefficient exists for DNA shear breakage. Changing the temperature from 25°C to 1°C required doubling the shear stress to achieve a similar rate. More detailed experiments, presented in Table III, show the change in breakage probability with temperature at constant shear stress over three temperature ranges.

Measurements of the temperature coefficient at constant shear stress gave unreasonably large values for the calculated activation energy for temperature ranges below 20°C. These data are also presented in Table III. An activation energy of 117 kcal/mole, as measured

Table II

The Dependence of Breakage Rate on Shear Stress

Temp (°C)	G_m (sec^{-1})	ηG_m (dynes/cm^2)	$\langle P \rangle \times 10^3$	$k(G_m)$ (sec^{-1})	$\left(\frac{d \ln \langle P \rangle}{d \ln G_m}\right)_T$	$\left(\frac{d \ln k(G_m)}{d(\eta G)}\right)_T$
10°C	99,800	1300	0.10	0.027		
10°C	107,300	1400	1.3	0.40	25	1.9×10^{-2} cm^2/dyne
10°C	116,000	1520	4.6	1.6		
25°C	81,200	726	0.097	0.012		
25°C	92,500	826	0.79	0.13	14	1.9×10^{-2} cm^2/dyne
25°C	103,000	921	2.6	0.52		

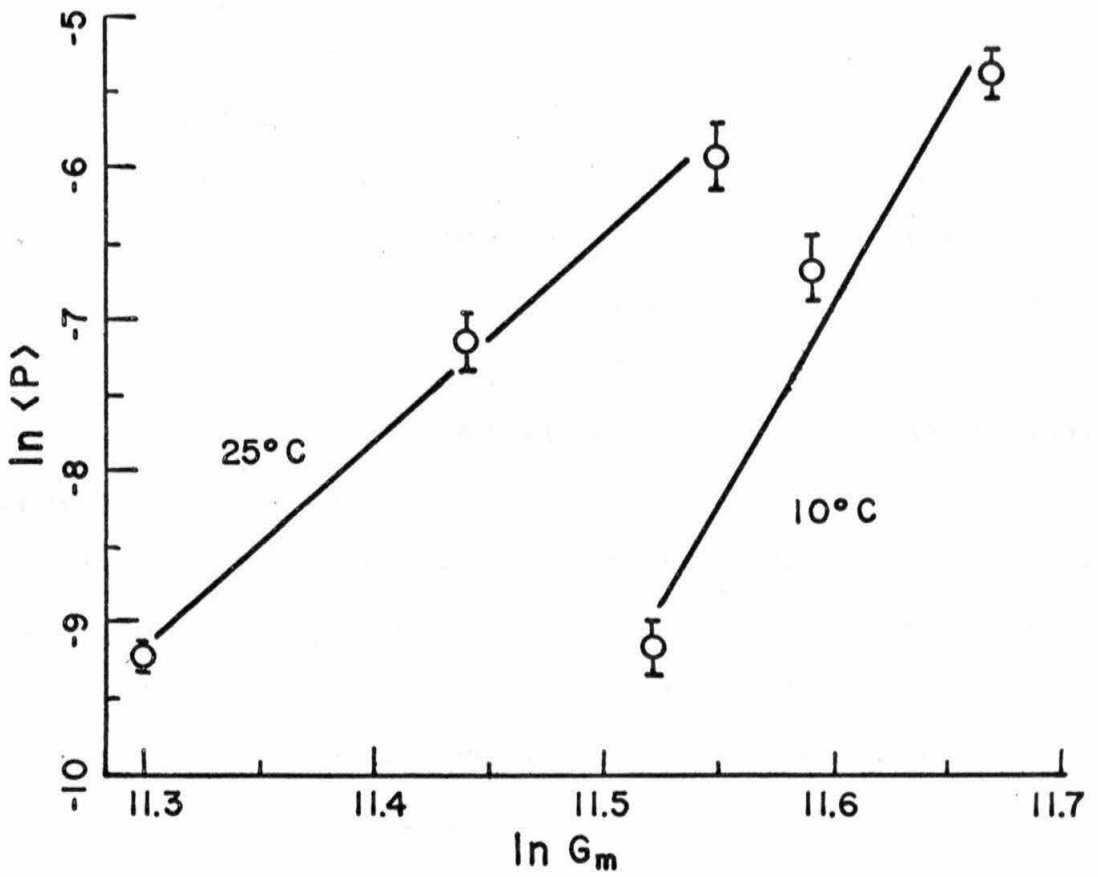

Fig. 8. This figure shows the dependence of the breakage probability, ⟨P⟩, on the maximum shear gradient, G_m, at two temperatures, 10°C and 25°C. The data for these plots are the same as those presented in Table II.

for the temperature interval 10°-15°C is unreasonable, to put it mildly, for a chemical reaction. We therefore searched for another explanation of the temperature variation of the rate.

The clue to the real source of the temperature coefficient arose from the flow dichroism work of Callis and Davidson.[24,25] They showed that while the mean extension of DNA in a flow field (and therefore the tensile force on the molecules) was proportional to ηG, the rate at which molecules relax from stretched-out configurations back to random coils was proportional to $1/\eta$ and independent of G. These observations are consistent with theories concerning flexible polymers in liquid velocity gradients.

We therefore suspected that if a process akin to relaxation were important in determining the breakage rate, the viscosity would be influential in ways other than as part of the shear stress. It soon became apparent that the observed temperature coefficient is entirely a result of the dependence of breakage rate on viscosity. Table IV lists three experiments in which the effects of changing the DNA solution viscosity by temperature and by sucrose addition are observed. Increasing the viscosity by a factor of two, whether by adding sucrose or lowering the temperature, necessitates increasing the shear stress by the same factor to obtain the same breakage rate. (The difference in breakage probabilities between the first and last experiments in Table IV is not significant. Identical probabilities could have been achieved if the shear stress were increased slightly in the sucrose experiment.)

Table III

The Effect of Temperature on Breakage Rate Measured at Constant Shear Stress

ΔT	$\left.\frac{\Delta \ell n \langle P \rangle}{\Delta T}\right)_{\eta G}$	$E_{act} \approx R \frac{\Delta \ell n \langle P \rangle}{\Delta(1/T)}$*
10°-15°C	0.72 deg^{-1}	117 kcal/mole
20°-25°C	0.31 deg^{-1}	54 kcal/mole
25°-30°C	0.17 deg^{-1}	37 kcal/mole

*The energy of activation is given by

$$E_{act} = R \frac{d \ell n k}{d(1/T)}$$

but this is approximately equal to $R \frac{d \ell n \langle P \rangle}{d(1/T)}$ because from Eq. (23),

$$\frac{d \ell n k}{d(1/T)} = \frac{d \ell n \langle P \rangle}{d(1/T)} + \frac{d \ell n}{d(1/T)} \left[\frac{d \ell n \langle P \rangle}{d \ell n G_m} + 3 \right]$$

If we look at the values given for $\left[\frac{d \ell n \langle P \rangle}{d \ell n G_m} + 3 \right]$ as a function of temperature, in Table II, we conclude

$$\frac{d \ell n \langle P \rangle}{d(1/T)} \gg \frac{d \ell n}{d(1/T)} \left[\frac{d \ell n \langle P \rangle}{d \ell n G_m} + 3 \right]$$

and that

$$\frac{d \ell n k}{d(1/T)} \approx \frac{d \ell n \langle P \rangle}{d(1/T)} \quad .$$

Table IV

The Dependence of Breakage Rate on Viscosity

Temp °C	$\eta/\eta H_2O, 25°C$	ηG_m (dynes/cm^2)	$\langle P \rangle \times 10^3$
25°C	1	920	2.1
1°C	1.94	2000	2.0
25°C	1.94*	2015	1.0

*20.5% sucrose (w/v).

Some conclusions derived in part from the viscosity data (see Discussion) suggested that the breakage rate per unit time might be a function of the residence time in the capillary. Table V presents a comparison of experiments in which all conditions are the same except for capillary length. Capillaries 2 and 3, as listed in Table I, are used for these experiments. The ratio of their lengths is 3.56.

There is an average relaxation time for setting up the steady state distribution of extended molecules in the flow field from which distribution the molecules have a certain rate of breakage. If this relaxation time is much less than the residence time of a molecule in the capillary, then the amount of breakage at a given shear gradient should be proportional to the residence time in the flow field, that is to the capillary length. Table V shows an additional increase of about a factor of two indicating that the relaxation time for effective extension is not short compared to the DNA's residence time in the 25 cm capillary. Implications of this observation will be considered in detail in the Discussion section.

The breakage probability in Table V marked with an asterisk is not completely reliable. The Reynolds number for this experiment, 2300, slightly exceeds the usual limit for non-turbulent flow. A more serious fault lies in the magnitude of the breakage probability. It exceeds the limit of 5×10^{-3} mentioned previously (see Experimental) as the condition for accurately assuming P(G), the breakage probability at G, is $\ll 1$ everywhere in the capillary. Nevertheless the results obtained

Table V

The Effect of Residence Time on the Breakage Rate

Capillary Length (cm)	ηG_m (dynes/cm^2)	$\langle P \rangle \times 10^4$	Ratio of Residence Times†	Ratio of Breakage Probabilities per Pass
25.3	920	26	3.64	6.4
90.0	920	166*		
25.3	725	0.97	3.58	7.9
90.0	725	7.7		

†End effect corrections have been applied; these are the residence times in the flow field.

*Re for this experiment was 2300.

from this experiment are confirmed by the more reliable experiment at the bottom of the table.

There are several shear breakage experiments which are not mentioned in this section because they are unimportant or irrelevant to any conclusions of this thesis. They may, however, contain useful information for other workers. A complete list of all successful shear breakage experiments appears in Appendix C.

DISCUSSION

Evaluation of a Possible Error

In laminar flow through a capillary, the residence time of a DNA molecule in a particular volume element is a function of the radial position of that volume element. The shortest residence time occurs for the solution passing down the axis of the capillary. The other extreme occurs at the capillary wall where the solution velocity approaches zero and the residence time approaches infinity. This characteristic of capillary flow introduces an opportunity for error in the calculation of breakage rates.

The breakage probability per pass at a given G is, by Eq. (11)

$$P(G) = 1 - e^{-k(G)t(r)} \tag{11}$$

which, due to the behavior of the quantity $k(G)t(r)$, is minimal in the capillary center and approaches unity at the capillary wall. Calculations of breakage rate constants (using Eq. (23)) are based on the assumption

$$k(G)t(r) \ll 1$$

which enabled us to rewrite Eq. (11) as

$$P(G) \approx k(G)t(r) \tag{18}$$

Clearly this assumption fails in some region near the capillary wall. If this region is sufficiently large and a significant fraction of the breakage

occurs in it, our calculated rate constants will be in error.

A solution to the problem is to design the breakage experiments so that the volume element next to the capillary wall in which $P(G) \approx 1$ is small and most of the breakage occurs in regions where $k(G)t(r) \ll 1$. These conditions are satisfied if the average breakage probability per pass, $\langle P \rangle$, is less than about 5×10^{-3}. This is shown by the following argument.

For laminar flow, the average breakage probability per pass is given by Eq. (17).

$$\langle P \rangle = \frac{4}{G_m^2} \int_0^{G_m} \left(1 - \frac{G^2}{G_m^2}\right) P(G) G \, dG \tag{17}$$

where

$$P(G) = 1 - e^{-k(G)t(r)} \tag{11}$$

The behavior of P(G) can be reasonably approximated by two relations:

$$\begin{aligned} &\text{for} \quad k(G)t(r) \leq 1, \quad P(G) = k(G)t(r) \\ &\text{for} \quad k(G)t(r) \geq 1, \quad P(G) = 1 \end{aligned} \tag{38}$$

The integral of Eq. (17) may then be divided into two integrals

$$\langle P \rangle \approx \frac{4}{G_m^2} \int_0^{G_1} \left(1 - \frac{G^2}{G_m^2}\right) k(G)t(r) G \, dG$$

$$+ \frac{4}{G_m^2} \int_{G_1}^{G_m} \left(1 - \frac{G^2}{G_m^2}\right) G \, dG \tag{39}$$

where G_1 is the gradient at which $k(G)t(r) = 1$. As before we notice that $t(r) = L/v(r)$ and letting $y = G/G_m = r/a$, Eq. (39) becomes

$$\langle P \rangle \approx \frac{8L}{aG_m} \int_0^{y_1} k(G) y \, dy + 4 \int_{y_1}^{1} (1-y_2) y \, dy \tag{40}$$

where now y_1 is the ratio of r/a at which $k(G)t(r)$ approaches unity.

The rate constant, k(G), may be written in terms of the shear gradient or y with the help of Eq. (23) derived in the Experimental section.

$$k(G_m) = \left(\frac{a}{8L}\right) \langle P \rangle G_m \left[3 + \frac{d \ln \langle P \rangle}{d \ln G_m}\right] \tag{23}$$

This relation should apply for arbitrary G. Rearranging and taking the natural logarithm,

$$\ln k(G) = \ln \langle P \rangle + \ln G + \ln \left[\left(\frac{a}{8L}\right)\left(3 + \frac{d \ln \langle P \rangle}{d \ln G}\right)\right] \tag{41}$$

If we neglect second derivatives and hold the temperature constant,

$$\left.\frac{d \ln k(G)}{d \ln G}\right)_T = \left.\frac{d \ln \langle P \rangle}{d \ln G}\right)_T + 1 \tag{42}$$

From the value of $(d \ln \langle P \rangle)/(d \ln G_m)$ at 25°C given in Table II, we conclude

$$d \ln k(G) = 15 \, d \ln G \tag{43}$$

or

$$k(G) = AG^{15} \quad \text{at } 25°C \tag{44}$$

where A is an integration constant. The magnitude of the exponent in this equation expresses the large observed variation in rate constant with a small change in shear gradient. We assume that for the range of G's important in a particular experiment, Eq. (44) applies. Therefore, from Eq. (40),

$$\langle P \rangle \approx \frac{8A\,L\,G_m^{14}}{a} \int_0^{y_1} y^{15}\, y\, dy + 4 \int_{y_1}^{1} (1-y^2) y\, dy \qquad (45)$$

or, introducing B for the constant $(2A\,L\,G_m^{14})/a$,

$$\langle P \rangle \approx 4B \int_0^{y_1} y^{16}\, dy + 4 \int_{y_1}^{1} (1-y^2) y\, dy \qquad (46)$$

These integrals may be evaluated to give

$$\langle P \rangle \approx \frac{4B\,y_1^{17}}{17} + (1-y_1^2)^2 \qquad \text{at } 25^\circ C \qquad (47)$$

where B and y_1 are still unknown.

Our purpose, in terms of Eq. (47), is to assess the relative contribution of the second term for various values of $\langle P \rangle$. This term represents the breakage occurring in the annulus next to the capillary wall in which $P(G) \approx 1$. For a given $\langle P \rangle$, the values of B and y_1 are found from Eq. (47) and the definition for y_1: $y = y_1$ when $k(G)t(r) = 1$. Or when

$$k(G)t(r) = \frac{2A\,L\,G^{15}}{aG_m(1-y_1^2)} = \frac{By_1^{15}}{(1-y_1^2)} = 1 \qquad \text{at } 25^\circ C \qquad (48)$$

Table VI shows the values of B and y_1 as a function of $\langle P \rangle$. The last column in the table gives the fractional contribution of the second term of Eq. (47) to $\langle P \rangle$. We conclude that for $\langle P \rangle \leq 5 \times 10^{-3}$, the approximation of Eq. (18) is reasonable at 25°C and Eq. (23) gives accurate values of $k(G_m)$.

Breakage in a Capillary

The extreme dependence of the breakage rate constant, k(G), on shear gradient (Eq. (44)) means that most of the breakage occurs fairly near the capillary wall where G reaches its maximum value. Figure 9(a) shows how the breakage probability increases with radius of flow through the capillary. The two curves shown are the breakage probability given by Eq. (11),

$$P(G) = 1 - e^{-k(G)t(r)} \tag{11}$$

and its approximation, Eq. (38).

$$\begin{aligned} &\text{for} \quad k(G)t(r) \leq 1, \quad P(G) = k(G)t(r) \\ &\text{for} \quad k(G)t(r) \geq 1, \quad P(G) = 1 \end{aligned} \tag{38}$$

The quantity k(G)t(r) is calculated in terms of the constant B and the variable, y.

$$k(G)t(r) = \frac{2A\,L\,G_m^{14} y^{15}}{a(1-y^2)} = \frac{By^{15}}{(1-y^2)} \quad \text{at } 25°C \tag{49}$$

Slightly different values for B are used in plotting Eqs. (11) and (38). The reason for the difference will be explained presently. Figure 9(a)

Table VI

Values of Equation (47) Constants B and y_1 for Several Magnitudes of $\langle P \rangle$

$\langle P \rangle$	B	y_1	$(1-y_1^2)^2 / \langle P \rangle$
0.0005	0.0022	0.999	0.01
0.0010	0.0043	0.998	0.02
0.0025	0.011	0.995	0.04
0.005	0.023	0.990	0.08
0.010	0.051	0.981	0.14
0.025	0.161	0.957	0.28
0.05	0.466	0.925	0.42

The numbers in this table are based on experimental data at 25°C for which $(d \ell n \langle P \rangle)/(d \ell n G_m) = 14$.

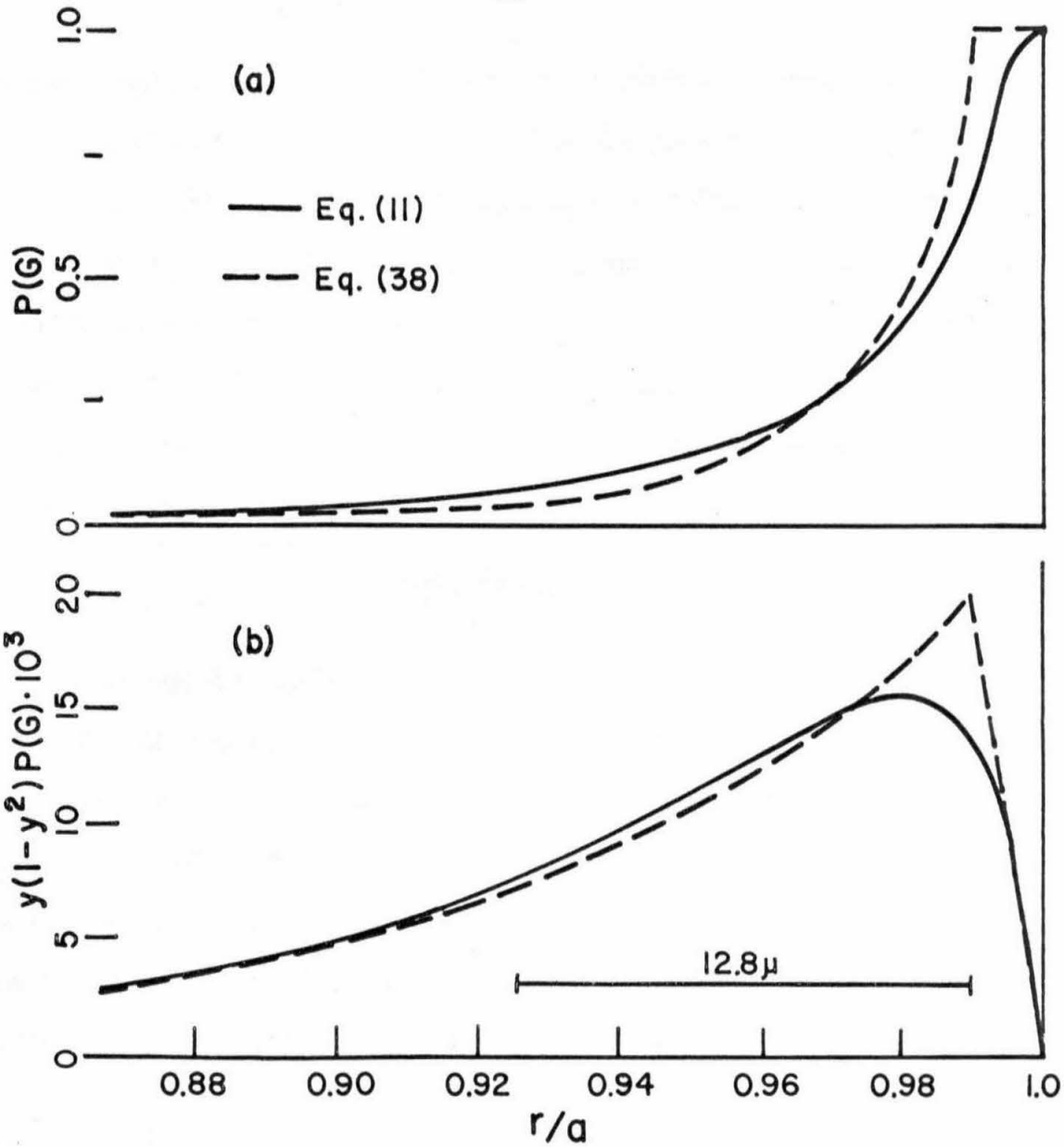

Fig. 9. Breakage probabilities are plotted versus radial distance from the capillary center. The abcissa for both figures, r/a, is the normalized radial distance from the center of the capillary. (a) shows breakage probabilities according to Eqs. (11) and (38). (b) shows those probabilities multiplied by the amount of material passing through each radial position (see text). These curves are based on a total probability of breakage per pass, $\langle P \rangle$, of 5×10^{-3} and a value of 14 for the quantity $(d\, \ell n \langle P \rangle / d\, \ell n\, G_m)$. The 12.8 μ length shown in (b) represents the contour length of $\lambda b_2 b_5 c$ DNA drawn to the scale of the figure when a, the capillary radius, is 0.02 cm.

demonstrates that most of the breakage probability occurs in the capillary annulus representing the outer 5% of the radius.

Figure 9(b) shows how the amount of breakage changes with radius of flow through the capillary. The amount of breakage per second at a given radius is the product of the breakage probability, P(G), and the amount of DNA flowing through the capillary per second at that radius, $2\pi r\, v(r)c\, dr$. Written in terms of y, the amount of breakage at a particular radius is

$$K(1-y^2)y\, P(G)$$

where K is equal to $\pi a^3 c\, G_m$ and is constant in any one pass. Figure 9(b) shows curves using P(G) as given by Equations (11) and (38). The curves have been drawn so that the areas under them, and therefore the total amount of breakage each represents, appear equal visually. The adjustments were made by using slightly different values for the constant B. It is apparent from Figure 9(b) that most of the breakage occurs in the outer 10% of the capillary radius.

Breakage Kinetics

In developing Eq. (23), with which one can calculate a breakage rate constant at a specific G, we assumed shear breakage was first order in the concentration of unbroken molecules (Eq. (9)). Indeed, almost all the shear breakage experiments seemed to follow first order kinetics. Plots of ℓnc, where c is the concentration of whole molecules, versus the number of passes gave straight lines. There were a few experiments whose kinetics were different from first order

in a specific way. In these experiments, the slope of the curve obtained from a ℓnc versus pass number plot decreased during the first 120 passes or so until it reached a steady minimum. Examples of such plots are given in Figures 6(c) and 7.

The 120 pass period, in which the slope changes, was termed the lag period since the probability of breakage lags behind its eventual steady state value during this time. The cause of the lag period phenomenon is unknown and little effort was expended trying to solve the problem once we learned how to avoid it. No lag period occurs when the DNA to be broken is first passed through the capillary about 200 times at a flow velocity too low to cause breakage. This procedure was originally adopted to convert hydrogen bonded circles and dimers to linear monomers prior to breakage. It had the additional effect of getting rid of the lag period.

Although we cannot pinpoint a cause for the lag period, we can eliminate several possibilities. The lag period is observed when a fraction of the DNA consists of hydrogen bonded circles at the outset of the experiment (Figure 6(c)). The circles are converted to linears in the first part of the experiment and might therefore influence the initial breakage rate. The principle objection to this explanation is that the circles are not present for the 120 pass lifetime of the lag period. We estimate that all the circles are pulled apart in the first 10 to 20 passes through the capillary.[26] A second objection is that the lag period is still observed when the DNA solution has been heated prior to breakage to dissociate the hydrogen bonded circles and dimers.

The lag period could arise from variations in self-protection during the experiment. Perhaps half molecules are less self-protective than intact ones. As more molecules are broken, self-protection decreases and breakage accelerates. If this were true, all breakage experiments should show a lag period since all are performed at DNA concentration at which self-protection is effective. This is not observed. Most breakage experiments show no lag period.

Figure 7 shows three experiments exhibiting lag periods. In these experiments, flow dichroism is used to measure the extent of breakage. The procedure for using this method of analysis involves passing the DNA solution through the titanium dichroism cell every fifth pass. Thus ample opportunity exists for the solution to pick up a few trace titanium ions which might accelerate the reaction rate by some catalysis mechanism. This proposal is discounted because the lag period is observed in other experiments in which no contact with metal occurred.

We also considered the possibility that the lag period is not artifactual at all but is a characteristic of the breakage reaction mechanism itself. One plausible hypothesis is that breakage occurs by consecutive single strand breaks as suggested by the diagram:

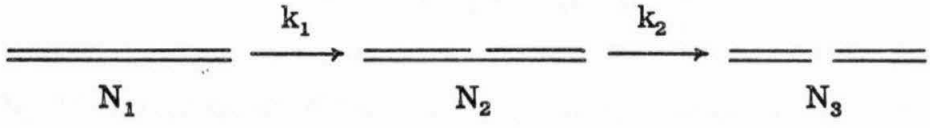

Then the kinetics treatment for consecutive reactions would apply. If the relative magnitudes of k_1 and k_2 are appropriate, a lag period would be observed. In the experiments which display no lag period, the DNA is first passed through the capillary to pull the circles apart and perhaps the first single strand break is introduced then.

In the diagram, N stands for the number of molecules of each type and k_1 and k_2 are the rate constants for the respective reactions. The rates of formation or disappearence of each species are

$$-\frac{dN_1}{dt} = k_1N_1 \tag{50}$$

$$\frac{dN_2}{dt} = k_1N_1 - k_2N_2 \tag{51}$$

$$\frac{dN_3}{dt} = k_2N_2 \tag{52}$$

The number of molecules of each species can be written in terms of the rate constants and time.

$$N_1 = N_0 e^{-k_1 t} \tag{53}$$

$$N_2 = \frac{N_0 k_1 e^{-k_2 t}}{(k_2-k_1)} \left[e^{(k_2-k_1)t} - 1\right] \tag{54}$$

$$N_3 = N_0 - (N_1+N_2)$$

$$= N_0\left[1 - \frac{k_2 e^{-k_1 t}}{(k_2-k_1)} + \frac{k_1 e^{-k_2 t}}{(k_2-k_1)}\right] \tag{55}$$

where N_0 is the number of molecules present initially.

If an appreciable quantity of the intermediate species exists, we will observe a different proportion of half molecules if the DNA is denatured than we will if it remains native. In band velocity sedimentation at neutral pH, the intermediate species appears to be a whole molecule. It would appear as one whole molecule and two halves in alkaline sedimentation.

Let us assign a weight of unity to whole molecules and a weight of 0.5 to halves. Then the weight fraction of whole molecules at neutral pH is

$$W_n = \frac{N_1+N_2}{N_1+N_2+2(0.5\,N_3)} = \frac{N_1+N_2}{N_0} \tag{56}$$

Similarly, the weight fraction of whole molecules at alkaline pH is

$$W_a = \frac{2N_1+N_2}{2N_1+N_2+2(0.5\,N_2)+4(0.5\,N_3)} = \frac{N_1+N_2/2}{N_0} \tag{57}$$

Using Eqs. (53), (54) and (55), we can plot W_n and W_a versus time for any ratio of the rate constants k_1 and k_2. Figure 10 displays several such plots. For comparison purposes, the experiment of Figure 6(c), which is a good example of the lag period, is replotted in Figure 10(a).

It is apparent from Figures 10(b), (d) and (f) that if $k_1 \geq k_2$, substantial differences in the fraction of intact molecules will be observed under the two sedimentation conditions. It is equally apparent from Figure 10(a) that no such differences do in fact occur at any time during an experiment.

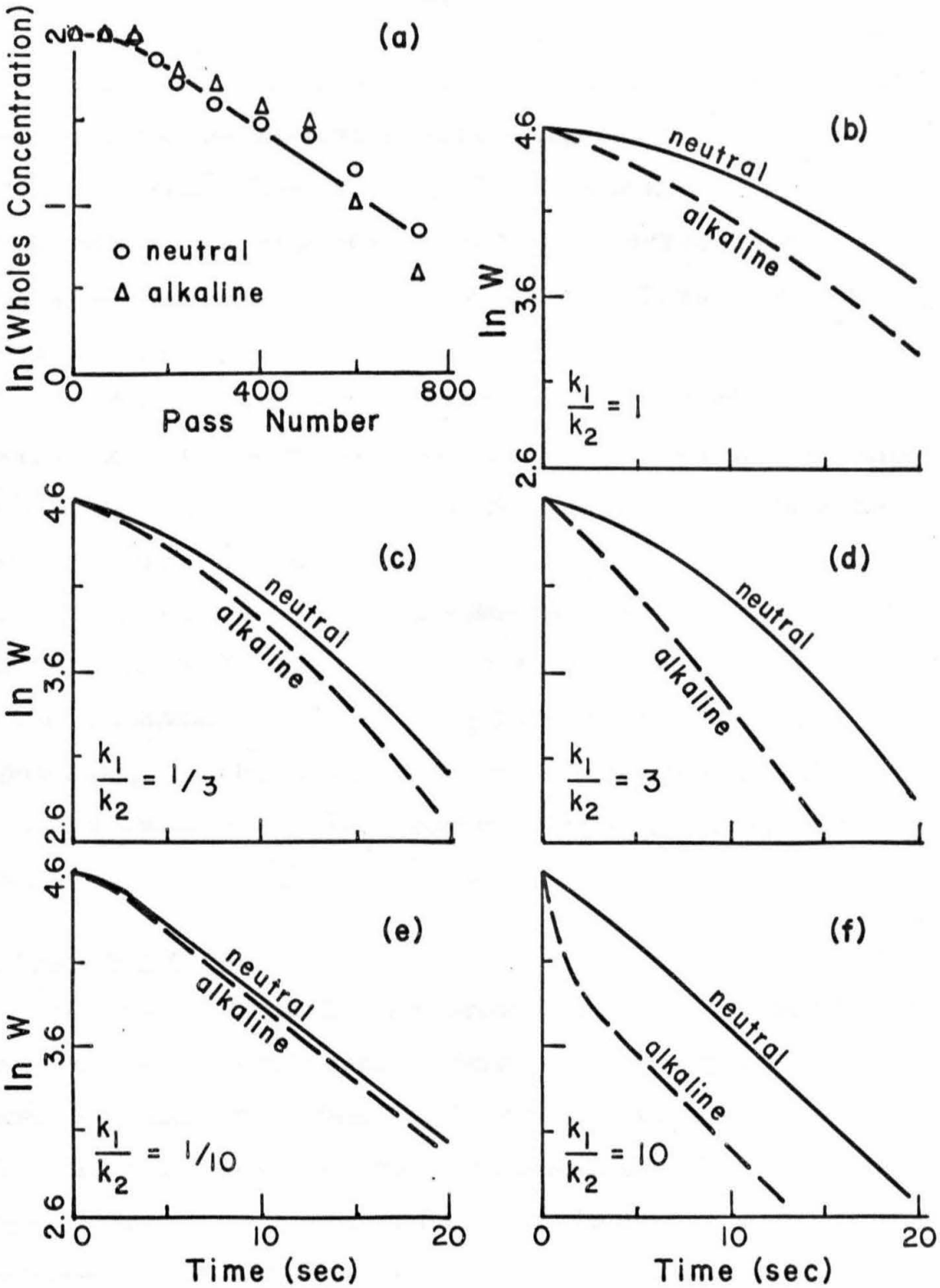

Fig. 10. This figure presents theoretical plots of the natural log of the wholes concentration ($\ell n W$) versus time for several values of the ratio k_1/k_2. See text for further explanation. (a) is a replot of Fig. 6(c).

As the value of k_1 decreases below that of k_2 (Figures 10(c) and 10(e)), the difference between neutral and alkaline whole molecule concentrations shrinks. When $k_1/k_2 = \frac{1}{3}$, $W_n - W_a$ is in the range of 0.1. This difference could be detected by the band velocity sedimentation technique as employed here. In the experiment of Figure 10(a), $W_n - W_a$ is less than 0.1.

We conclude that the experimental measurement of W_n and W_a, as in Figure 10(a), shows that if the reaction does occur by consecutive single strand breaks, $k_1/k_2 < \frac{1}{3}$. For all practical purposes then, the first step is rate determining.

The kinetics which accurately describe shear breakage then are first order and the lag period is due to some as yet undiscovered effect. We want to emphasize again that it is possible to get good kinetics, without a lag, if the Hershey circles and cohered dimers are dissociated by treatment with a lower shear gradient before commencing the experiment.

Critical Shear Stress

The idea of a critical shear stress seems intuitively sound since one would expect a certain minimum tensile force is required to break a bond. Our data indicate that if such a minimum force exists, it is below the forces normally generated in a breakage experiment. In the range of shear gradients used for this work, the breakage rate is a continuous function of the shear stress. In fact, if one extrapolates a plot of breakage rate versus shear stress to zero rate, the kind of curve shown in Figure 11 results. The approach to zero rate appears

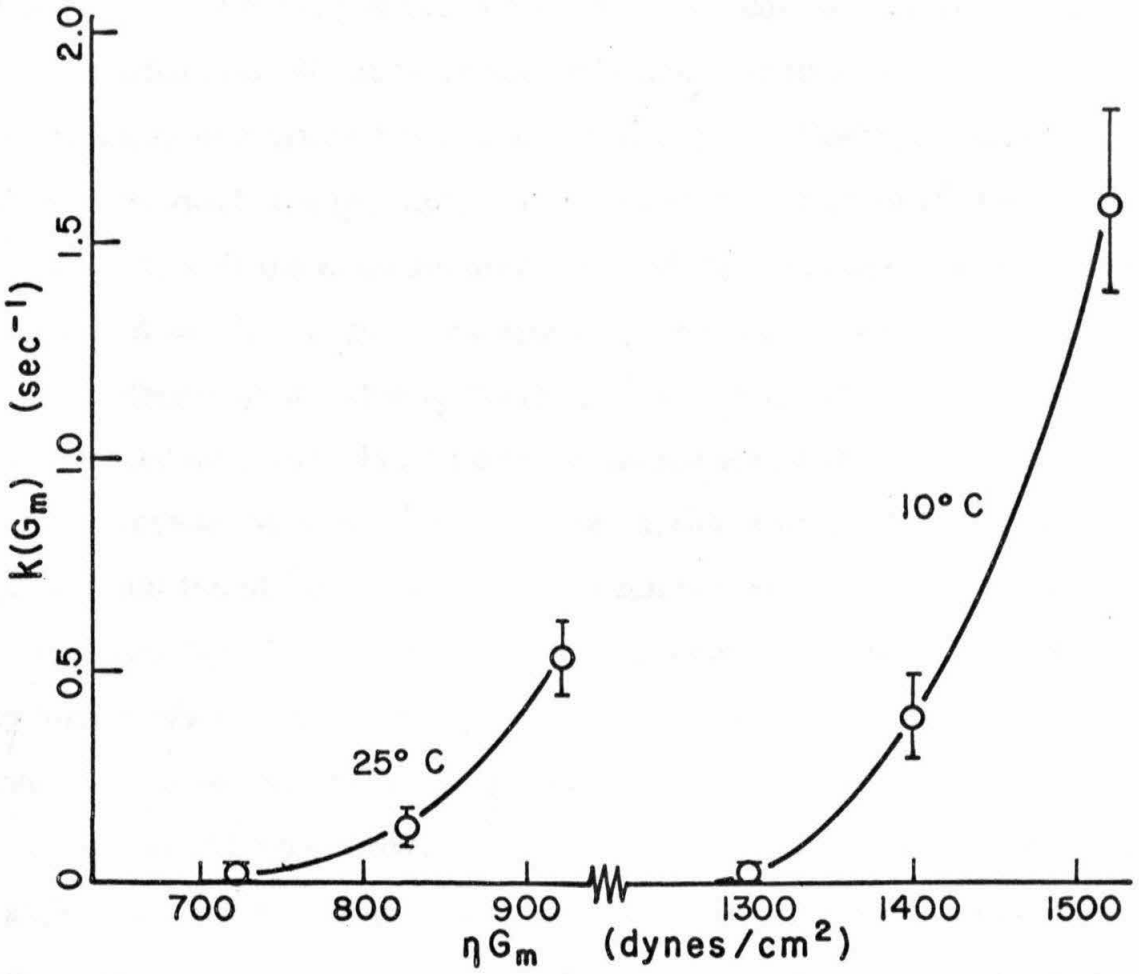

Fig. 11. The breakage rate constants of Table II are plotted versus shear stress. The curves through the points appear to extrapolate to zero rate asymptotically.

asymptotic.

Other workers have tried to measure critical shear stresses for DNA.[3,4,5] We suggest the concept of a critical shear stress is an oversimplification. We observe the breakage rate to be a continuous monotonically increasing function of shear stress. Observations of critical flow rates are probably due to two characteristics of shear breakage. One is the extreme sensitivity of the breakage rate to shear gradient. A small change in the speed of a rotating blade can produce dramatic effects on the rate of breakage. The other characteristic is demonstrated by Figure 11. The figure shows a plot of the rate constant, k, versus the shear stress at the capillary wall, ηG_m. It is apparent that the slope of the curve through the points, $dk/d\eta G_m$, is not constant. It is larger at relatively high breakage rates. Thus if only high breakage rates are observed, one might think the plot of k versus ηG_m does extrapolate to zero rate.

It should be mentioned that since $dk/d\eta G_m$ is not constant, the straight lines drawn in Figure 8 are somewhat misleading. It would be more accurate to draw curves through the points whose slopes increase with decreasing G_m. However, in view of the sparseness of the experimental data, we must take the straight lines as at least a reasonable approximation of the dependence of the breakage rate on shear gradient for the interval shown.

Self-Protection

The self-protection phenomenon was one of the first characteristics of shear breakage to be observed.[3,9] It is documented in this

work by Figure 4. A specific mechanism for this phenomenon has not been proposed but the information at hand permits us to describe a crude model.

Figure 4 shows self-protection is operative for breakage of linear $\lambda b_2 b_5 c$ DNA at a DNA concentration of 0.5 μg/ml. At this concentration, each molecule has, on the average, about 8×10^{-11} cc to move around in without physically encountering its neighbors. Let us take the volume of a sphere with radius equal to the radius of gyration for $\lambda b_2 b_5 c$ DNA as a reasonable estimate of the volume occupied by a molecule in an average random coil configuration. Such a sphere has a volume of 3×10^{-13} cc, almost 300 times smaller than the volume available to the molecule in a breakage experiment. Assuming that intermolecular contact or near contact plays an essential part in self-protection, molecules participating in the phenomenon must have an effective volume much larger than that of an average random coil molecule. This conclusion is consistent with the model for breakage (presented below) in which the molecules of a population which are broken are in an exceptionally extended configuration. In terms of this model, self-protection serves to inhibit the formation of extended molecules.

Temperature and Viscosity Effects.

It was evident from very early experiments that the shear breakage rate in a capillary exhibits a large temperature dependence. We believed it arose from the effect of temperature on the rate of a thermal hydrolysis which is facilitated by shear stress. We therefore performed

a series of experiments designed to measure an activation energy of the thermal hydrolysis reaction in the presence of shear. The experiments consisted of measuring the breakage probability, ⟨P⟩, at various temperatures, holding the shear stress, ηG, constant. From Eq. (6) we recall that ηG is constant at constant nitrogen pressure.

$$\eta G_m = \frac{Pa}{2L} = \frac{4V\eta}{\pi a^3} \tag{6}$$

As the temperature drops, the viscosity of the solution, η, increases. But if the driving nitrogen pressure is held constant, the effect of higher viscosity is to reduce the flow velocity and the product of viscosity times shear gradient remains constant.

Table III shows 5° variations in temperature induce appreciable changes in ⟨P⟩ measured at constant ηG. The table also gives some energies of activation based on the same experiments. The activation energies obtained from experiments near room temperature (about 45 kcal/mole) are plausible for a solvolysis reaction. The activation energy for hydrolysis of the diester linkage in dipropyl phosphate ($0 \leq$ pH ≤ 1.24, $100.3°C \leq T \leq 133.3°C$) is 27.3 kcal/mole.[27] However, below room temperature the observed activation energies for DNA shear breakage are unreasonably large (e.g., 117 kcal/mole at 10° to 15°C). It was apparent that the observed variation of breakage rate with temperature cannot arise from the influence of temperature on a thermal hydrolysis reaction.

Our search for an alternative explanation included a look at the effects of salt concentration on breakage rate. The observed temperature

coefficient for shear breakage could occur if local denaturation were the rate limiting step. Since denaturation is facilitated by low salt concentrations, this hypothesis is easily tested. In the experiment of Figure 6(a), the total sodium ion concentration is 0.1 F, in Figure 6(b), it is 0.016 F. In terms of DNA melting behavior, this factor of six change in salt concentration is about equivalent to a 14°C change in temperature.[28] It is evident from the figure that no change in the breakage rate was observed in these two experiments. From previous discussion we know a 14°C change in temperature would induce greater than a 10-fold variation in the probability of breakage, ⟨P⟩. We conclude that local denaturation is not involved in the rate determining step of shear breakage.

An insight as to the real cause of the shear breakage temperature coefficient arose from the work of Callis and Davidson.[24,25] Their investigations showed that while the steady state orientation of DNA molecules in a liquid velocity gradient depends on the shear stress, ηG, the time for relaxation of extended molecules back to random coils is inversely proportional to the viscosity of the solution, η. These considerations suggested the model to be described below in which, at constant shear stress, ηG, the reaction rate is inversely proportional to the viscosity. As we shall now see, the experimental data agree with this prediction. We will further observe that the temperature coefficient of the reaction rate <u>at constant shear stress</u> is entirely due to the temperature coefficient of the solvent viscosity and the variation of reaction rate with viscosity.

Examination of the data already presented in Table IV shows that the effect of lowering the temperature was solely to increase the viscosity. The table shows that whether the viscosity is raised by adding sucrose or by lowering the temperature, the effect is the same.

We returned to our previous valuation of the breakage temperature coefficient measured at constant ηG (Table III) and found that these data confirm the conclusion drawn from the viscosity study in the following way. The force tending to extend a molecule in a liquid velocity gradient is proportional to the velocity of the liquid relative to the molecule (represented by G) and to a frictional coefficient which contains a viscosity factor. The speed at which a molecule unfolds from a random coil to an extended configuration would be proportional to this force and thus to ηG. Simultaneously, the unfolding rate is inversely proportional to the viscosity since the unfolding motion is resisted by the viscosity of the solution. Therefore the breakage rate, k, will be some function of ηG and simultaneously inversely proportional to the viscosity, η.

$$k = \frac{f(\eta G)}{\eta} \tag{58}$$

where f denotes an unknown function. Let us express the breakage temperature coefficient measured at constant ηG as $dk/dT)_{\eta G}$, or

$$\left(\frac{dk}{dT}\right)_{\eta G} = \left(\frac{dk}{dG}\right)_{T} \left(\frac{dG}{dT}\right)_{\eta G} \tag{59}$$

The last factor in Eq. (59) can be rewritten using $\eta G/\eta$ for G.

$$\left.\frac{dG}{dT}\right)_{\eta G} = \left.\frac{d(\eta G/\eta)}{dT}\right)_{\eta G} = -\left.\frac{G d\eta}{\eta dT}\right)_{\eta G} \tag{60}$$

Substituting into Eq. (59),

$$\left.\frac{dk}{dT}\right)_{\eta G} = -\left.\frac{dk}{dG}\right)_{T} \frac{G}{\eta}\left.\frac{d\eta}{dT}\right)_{\eta G} \tag{61}$$

or

$$\left.\frac{d\,\ell n\,k}{dT}\right)_{\eta G} = -\left.\frac{d\,\ell n\,k}{d\,\ell n\,G}\right)_{T} \left.\frac{d\,\ell n\,\eta}{dT}\right)_{\eta G} \tag{62}$$

Values for the quantity on the left side of Eq. (62) are given in Table III, * the variation of breakage rate with shear gradient at constant

---

*From Eq. (23),

$$\ell n\,k = \ell n\,\langle P\rangle + \ell n\,G + \ell n\left[\frac{a}{8L}\left(3 + \frac{d\,\ell n\langle P\rangle}{d\,\ell n\,G}\right)\right]$$

$$\left.\frac{d\,\ell n\,k}{dT}\right)_{\eta G} = \left.\frac{d\,\ell n\langle P\rangle}{dT}\right)_{\eta G} + \left.\frac{d\,\ell n\,G}{dT}\right)_{\eta G} + \frac{d\,\ell n\,(3 + d\,\ell n\langle P\rangle/d\,\ell n\,G)}{dT}$$

since

$$\left.\frac{d\,\ell n\,(\eta G/\eta)}{dT}\right)_{\eta G} = -\left.\frac{d\,\ell n\,\eta}{dT}\right)_{\eta G}$$

$$\left.\frac{d\,\ell n\,k}{dT}\right)_{\eta G} = \left.\frac{d\,\ell n\langle P\rangle}{dT} - \frac{d\,\ell n\,\eta}{dT}\right)_{\eta G} + \frac{d\,\ell n\,(3 + d\,\ell n\langle P\rangle/d\,\ell n\,G)}{dT}$$

and since

$$\left.\frac{d\,\ell n\langle P\rangle}{dT}\right)_{\eta G} \gg \left.\frac{d\,\ell n\,\eta}{dT}\right)_{\eta G} \quad \text{and} \quad \frac{d\,\ell n\,(3 + d\,\ell n\langle P\rangle/d\,\ell n\,G)}{dT}$$

$$\left.\frac{d\,\ell n\,k}{dT}\right)_{\eta G} \approx \left.\frac{d\,\ell n\langle P\rangle}{dT}\right)_{\eta G}$$

temperature is given in Table II and the change of viscosity with temperature is obtainable from handbooks. These quantities were used to construct Table VII below. It demonstrates the validity of Eq. (62) for two temperature ranges, 10°-15°C and 20°-25°C. Thus our temperature coefficient for breakage at constant ηG is in fact the effect of temperature on the viscosity of the solution, and the effect of viscosity on the breakage rate at constant shear stress.

Table VII

Experimental Verification of Equation (62)

ΔT	$\frac{\Delta \ell n k}{\Delta T}\Big)_{\eta G}$	$-\left[\frac{d \ell n k}{d \ell n G}\Big)_{T} \times \frac{\Delta \ell n \eta}{\Delta T}\Big)_{\eta G}\right]$
10°-15°C	0.72 deg^{-1}	0.73 deg^{-1}
20°-25°C	0.31 deg^{-1}	0.37 deg^{-1}

We conclude that our attempts to determine the effects of temperature on the chemistry of breakage were unsuccessful, but they lead to the elucidation of the very important relation between breakage rate and viscosity.

We now present a model for shear breakage which the foregoing data suggest. When the DNA just enters the capillary, it is in a random coil configuration represented by A below. As it travels through the capillary near the wall, it is distorted into extended configurations B and C until it breaks, D.

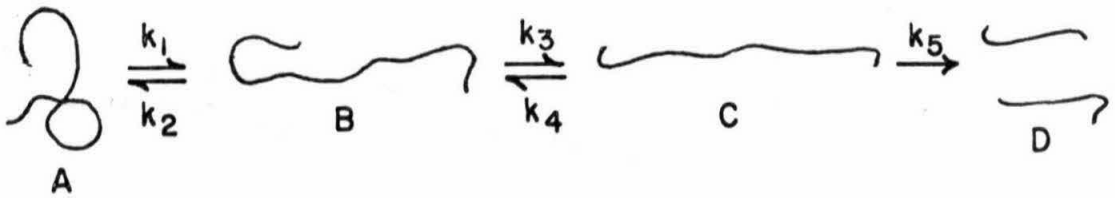

The configuration A represents the average relaxed random coil with an end-to-end distance typical of molecules in a static solution. B represents the average extended random coil in the given capillary shear gradient. Its degree of extension or end-to-end distance is typical for molecules in this particular flow field. The configuration C represents a fluxuation from the average state B. Although B represents the most probable extension for molecules in this shear gradient, there will be a certain number of molecules of the C type having more than the average degree of extension. It is from this small population of molecules that half molecules are formed.

Under steady state conditions,

$$(k_2 + k_3)B = k_1A + k_4C \tag{63}$$

and

$$(k_4 + k_5)C = k_3B \tag{64}$$

where the letters A, B, C, and D now stand for the concentrations of molecules in the respective states. The observed rate of breakage is

$$\text{Rate} = k_5C \tag{65}$$

which may be written in terms of all the rate constants using Eqs. (63) and (64):

$$\text{Rate} = \frac{k_3 k_5 B}{(k_4+k_5)} = \frac{k_3 k_5}{(k_4+k_5)} \left[\frac{k_1(A+B)}{(k_2+k_3)\left(1 - \frac{k_3 k_4}{(k_2+k_3)(k_4+k_5)}\right) + k_1} \right] \tag{66}$$

In our view of the breakage process, once a molecule reaches the highly extended configuration (represented by C in the reaction scheme above) breakage is almost certain. For such a molecule, the tensional forces applied to it by the moving liquid are ample for pulling the DNA backbone apart. This means that $k_5 \gg k_4$. We can then simplify Eq. (66) to give

$$\text{Rate} \approx \frac{k_1 k_3 (A+B)}{(k_2+k_3)\left(1 - \frac{k_3 k_4}{k_5(k_2+k_3)}\right) + k_1} \tag{67}$$

We also know that reaching extension C is a fairly unlikely event. Experiments are designed such that less than one molecule in 200 is broken per pass. That is, most of the molecules are in the equilibrium between A and B as they tumble through the capillary. In terms of our model then, $k_2 \gg k_3$, and the normalized rate becomes,

$$\frac{\text{Rate}}{(A+B)} \approx \frac{k_1 k_3}{k_2\left(1 - \frac{k_3 k_4}{k_2 k_5}\right) + k_1} \tag{68}$$

Since the ratios k_3/k_2 and k_4/k_5 are both less than unity, we may ignore the term k_3k_4/k_2k_5 in Eq. (68) which then reduces to

$$\frac{\text{Rate}}{(A+B)} \approx \left(\frac{k_1}{k_1+k_2}\right) k_3 \tag{69}$$

If we look at Eq. (69) and the model depicted on page 69, we recognize this is now the familiar steady-state reaction rate equation in which B is in quasi-equilibrium with A and the reaction rate is the rate at which B-type molecules go to C-type molecules. Every C-type molecules breaks. The constant $k_1/(k_1+k_2)$ is the equilibrium ratio $B/(A+B)$. The B-type molecules are the extended molecules which give rise to flow dichroism. Thus, since both theoretically and experimentally, the flow dichroism is a function of the shear stress, ηG, the ratio $k_1/(k_1+k_2)$ is predicted to be a function of the shear stress. The rate constant k_3 should also depend on the shear stress, but it is a rate constant for the extension of a macromolecule in a viscous fluid and so, at constant shear stress, it is inversely proportional to the solvent viscosity η. Thus, we see that the reaction rate at the steady state is some function of shear stress, and at constant shear stress is inversely proportional to viscosity.

Note further that the equation discussed so far is for the steady-state rate. If we start with all molecules in state A and then suddenly apply the flow field, it is a characteristic result for this kind of kinetics that the relaxation time for reaching the steady state is $1/(k_1+k_2)$. For the reasons already discussed, this is also the characteristic relaxation time for establishing flow dichroism when molecules suddenly enter a flow field.

The flow dichroism relaxation time measurements for $\lambda b_2 b_5 c$ DNA performed by Callis and Davidson[25] give a relaxation time of 0.03 sec. for the decay of flow dichroism when the flow is stopped. This is the constant $1/k_2$. Callis and Davidson give arguments indicating that k_2 is probably somewhat greater than k_1 and that the relaxation time for establishing flow dichroism, $1/(k_1+k_2)$, is not much shorter than the relaxation time for its decay. We conclude that the characteristic time for establishing a steady-state breakage rate in the capillary should be 0.03 sec. or less.

In anticipation of the next section, the latter feature of this kinetic model predicts that if the residence time of the DNA in the capillary is shorter or comparable to $1/(k_1+k_2)$, then the rate of breakage per second will be affected by a change in the residence time. Alternatively, if the residence time is much longer than $1/(k_1+k_2)$, we would expect a change in residence time to have little or no effect on the breakage rate.

Capillary Length Effect

In the previous section, we showed the rate limiting step for shear breakage is the rate at which DNA molecules unfold. It is interesting to ask how the time constant for unfolding compares with the time the DNA spends in the capillary. Is steady state breakage established in the time it takes the DNA to flow through?

For a typical breakage experiment, the shear gradient at the capillary wall is about 10^5 sec^{-1}. Using Eq. (1), we calculate the linear

flow velocity of the fluid at the radius where DNA is broken (r/a = 0.95; see Figure 9) to be about 95 cm/sec. Therefore, DNA broken in our 25 cm long capillary spends about 0.25 sec. in the presence of shear forces.

From the work of Callis and Davidson on the hydrodynamic relaxation behavior of DNA,[25] we consider 0.03 sec. a reasonable time for a $\lambda b_2 b_5 c$ DNA molecule to unfold from a random coil to an extension required for breakage. This is the slowest relaxation time measured by Callis and Davidson for this DNA and it is independent of the magnitude of the shear gradient used to extend the molecules.

Since 0.03 sec. is short compared to the DNA's residence time (at r/a = 0.95), we expect steady state breakage is established before the DNA issues from the end of the capillary. Our expectations are confirmed by a combination of experimental evidence and theoretical considerations; though, as we shall see, a time somewhat longer than the 0.03 sec. relaxation time is probably required to reach a steady breakage rate.

Table V presents the results of experiments designed to measure the effect of residence time on the rate of breakage. Two capillaries are used, one 25 cm. long and one 90 cm. long (see Table I for complete specifications). Ignoring end effect corrections, their ratio of lengths is 3.56. Experiments were performed in the two capillaries such that all conditions were the same except for the residence time. To obtain equal shear stresses, a small increase in flow rate was required for the longer capillary because of its slightly larger

radius. From Table I we calculate G_m will be the same in each capillary if $V_{90} = 1.14\ V_{25}$ where V is the volume flow rate in ml./sec.

The data in Table V show that changing the residence time (at r/a = 0.95) from 0.33 sec to 1.14 sec has the effect of multiplying the probability of breakage per pass by about 7. We infer that a substantial portion of the 0.33 sec residence time in the shorter capillary is required to approach steady state breakage. If a steady rate were achieved in say 0.03 sec or so, we would expect the ratio of breakage probabilities in the two capillaries to approximate their ratio of residence times for these experiments.

To examine the behavior of the breakage rate at early times (0 to 0.3 sec) and to get an idea of how long it takes for breakage to reach a steady state, we formulated a one-dimensional theoretical model:

We consider the simple case of a dumbbell consisting of two spheres of equal size and mass connected by a massless spring. The distance between the centers of the spheres is 2ℓ. The dumbbell is in a uniform liquid velocity gradient. The liquid moves in the x direction with a velocity v(z) and the shear gradient, -dv(z)/dz is a constant, G. We visualize the dumbbell moving along with the liquid at a velocity equal to the velocity of the liquid at the dumbbell's center of mass. If we let the origin of our coordinates be the dumbbell's center of mass, v(z) becomes the liquid velocity relative

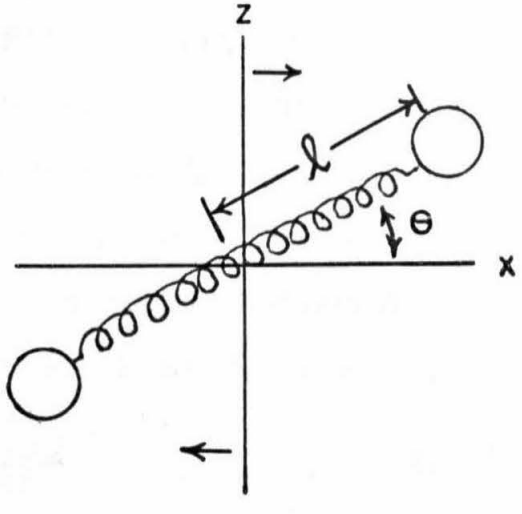

to the dumbbell. The arrows in the figure above indicate directions of the relative fluid velocity v(z).

To simplify the problem, we will only consider the behavior of the x-projection of the dumbbell and we ignore rotation of the dumbbell in the x-z plane. By treating only the x-projection, we reduce the problem to a one-dimensional one. It was desirable in the beginning to speak in terms of two dimensions to show the origin of the tensile force exerted on the dumbbell by the moving liquid. The magnitude of the force at one end is $\rho v(z')$ where ρ is a frictional coefficient and $v(z')$ is the fluid velocity at $z' = \ell \sin\theta$. In our one-dimensional treatment, we will call the stretching hydrodynamic force ρv_f (where $v_f = v(z')\cos^2\theta$).

The restoring force exerted by the spring on the end of the dumbbell is $-kTx/b^2$ where the Hooke's Law force constant is kT/b^2. The quantity b is a fundamental dimension of the problem. It is the average distance from the origin to the sphere at the end of the dumbbell in the absence of hydrodynamic flow. It results from a balance between Brownian motion "randomizing" forces and the spring's restoring force. A dumbbell the size of DNA molecules will act as though there is a force on each end equal to $-kT\,\partial \ell n \psi / \partial x$ through the influence of Brownian motion. Here $\psi(x, t)$ is the probability that the end of the dumbbell will be found between x and $x + dx$ at time t.

If we now combine the hydrodynamic, spring and Brownian motion forces, the total force on one end of the dumbbell, f, is

$$f = \rho v_f - \frac{kT}{b^2} x - kT \frac{\partial \ell n \psi}{\partial x} \qquad (70)$$

The equation of motion for the dumbbell end (relative to its center of mass) is then

$$\frac{dx}{dt} = v_f - \frac{kT}{\rho b^2} x - \frac{kT}{\rho} \frac{\partial \ell n \psi}{\partial x} \tag{71}$$

Introducing the equation of continuity,

$$\frac{\partial \psi}{\partial t} = - \frac{\partial}{\partial x} \left(\psi \frac{dx}{dt} \right) \tag{72}$$

we arrive at the differential equation whose solution will describe the motion of the dumbbell end subject to the boundary conditions we impose:

$$\frac{\partial \psi}{\partial t} = - \frac{\partial}{\partial x} \left[\psi v_f - \frac{kT}{\rho b^2} \psi x - \frac{kT}{\rho} \frac{\partial \psi}{\partial x} \right] \tag{73}$$

We notice immediately that in the absence of flow, the quantities $\partial\psi/\partial t$ and v_f in Eq. (73) vanish and

$$\frac{\partial \psi}{\partial x} = - \frac{\psi x}{b^2} \tag{74}$$

This situation occurs before the dumbbell enters the capillary. The solution to Eq. (74) is our boundary condition at $t = 0$,

$$\psi(x, 0) = \frac{1}{\sqrt{2\pi}} e^{-x^2/2b^2} \tag{75}$$

This expression for the probability function, ψ, describes the conformation of a random coil polymer in a static solution.

Upon entering the capillary, the dumbbell is in the presence of a uniform velocity gradient and its distortion is governed by Eq. (73). We impose a second boundary condition which demands that when the dumbbell is stretched to a certain critical extension, x_c, it breaks.

$$\psi(x_c, t) = 0, \qquad x_c > 0 \tag{76}$$

We will let the fluid velocity, v_f, be the mean displacement of the dumbbell end from the origin times the shear gradient.

$$v_f = Gb \tag{77}$$

Then Eq. (73) becomes

$$\frac{\partial \psi}{\partial t} = \frac{kT}{\rho} \frac{\partial^2 \psi}{\partial x^2} + \left(\frac{kT}{\rho b^2} x - Gb \right) \frac{\partial \psi}{\partial x} + \frac{kT}{\rho b^2} \psi \tag{78}$$

We have not attempted an exact solution to this differential equation consistent with the boundary conditions of Eqs. (75) and (76). Our simple model resembles the real case of DNA in a liquid velocity gradient so remotely that we considered the time investment required to solve Eq. (78) unjustified. However, some of the salient features of the model become apparent with a little manipulation.

By removing the boundary condition given by Eq. (76), Eq. (78) has the solution

$$\psi(x, t) = \frac{1}{\sqrt{2\pi}} \exp\left\{ -\tfrac{1}{2} \left[\frac{x}{b} - \frac{\rho G b^2}{kT} \left(1 - e^{-t/\tau}\right) \right]^2 \right\} \tag{79}$$

where $\tau = \rho/kT$.* This solution describes a Gaussian distribution with a standard deviation b and maximum $1/\sqrt{2\pi}$ for all values of t. The center of the distribution begins at the origin at t = 0 and asymptotically approaches $\rho Gb^3/kT$ at $t = \infty$. The distribution does not change shape during the migration. Equation (79) is plotted in Figure 12 for several values of t. To draw these curves, we have assumed the time constant for stretching the dumbbell is the same as the hydrodynamic relaxation time for $\lambda b_2 b_5 c$ DNA measured by Callis and Davidson, 0.03 sec. We have taken b equal to one-half the root mean square end to end distance of $\lambda b_2 b_5 c$ DNA as a random coil. Thus we take $b = 0.5\,\mu$.

We see from Eq. (79) that $\rho Gb^3/kT$ is constant for constant G and is the displacement of the dumbbell end from the origin at infinite time. It is the position of the center of the Gaussian distribution of Figure 12 when it has moved to its steady state location. A reasonable estimate for the value of this constant can be obtained from measurements of the steady state dichroism of $\lambda b_2 b_5 c$ DNA. The details of the calculation are given in Appendix E. It is based on the relation

$$\frac{\Delta A}{A} = \tfrac{3}{4}\left(\langle\cos^2\theta\rangle - \tfrac{1}{3}\right) \qquad (80)$$

---

*We are indebted to Professor Donald Cohen for his invaluable help in leading us to this solution.

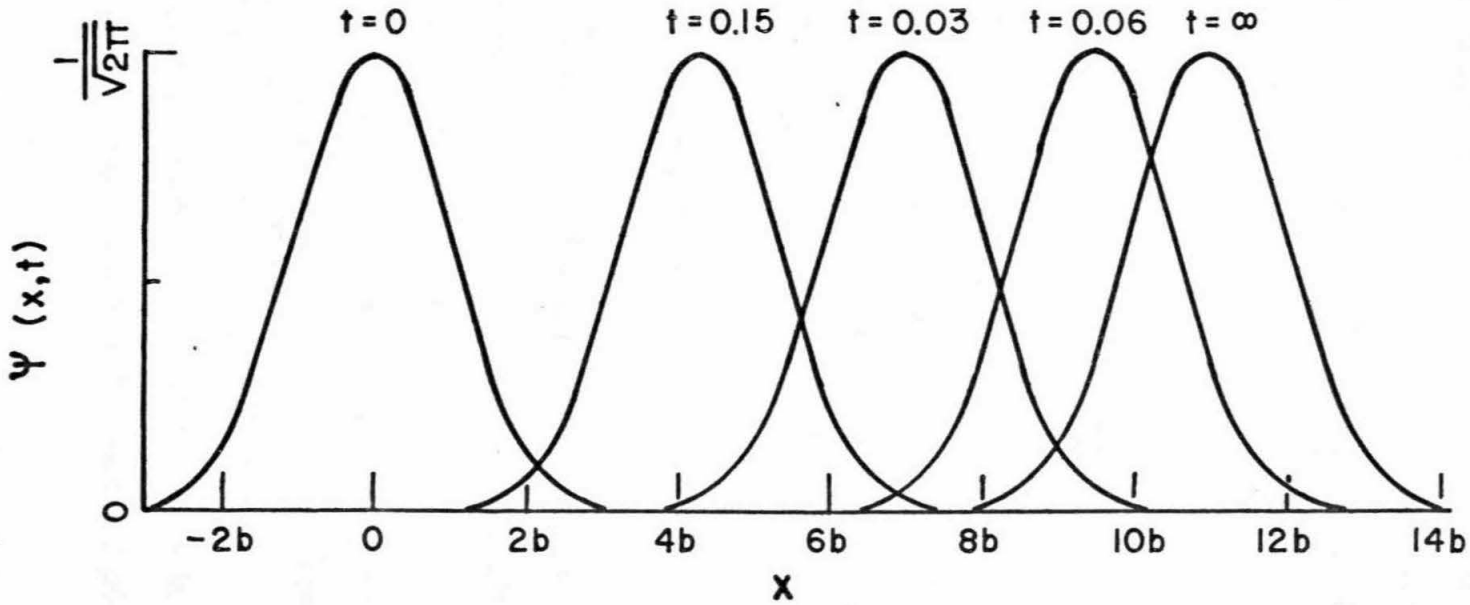

Fig. 12. The position of the dumbbell end relative to its center of mass given by Eq. (79) is plotted versus distance at several times after it "enters" the flow field. The time values given are in seconds. Constants $\rho Gb^3/kT$ and τ used in the plots are respectively 5.5 μ and 0.03 sec.

in which dichroism, $\Delta A/A$, is given in terms of the average cosine (squared) of the angle between statistical segments of the DNA chain and an optical axis. From the treatment of the relation between elastic constants and stress birefringence of elastic substances by Kuhn and Grün[29] we can derive a relation between $\langle \cos^2 \theta \rangle$ and the most probable end to end distance, h.

$$\langle \cos^2 \theta \rangle = 1 - \frac{2}{\beta} \left(\frac{h}{NA} \right) \tag{81}$$

where N is the number of statistical segments in the DNA and A is the length of each segment. N = 160 for $\lambda b_2 b_5 c$ DNA where A is taken to be 800 Å. Beta is a Lagrange multiplier which may be evaluated from the relation

$$\langle \cos^2 \theta \rangle = 1 - \frac{2 \coth \beta}{\beta} + \frac{2}{\beta^2} \tag{82}$$

Callis and Davidson[24] estimate the dichroism of $\lambda b_2 b_5 c$ DNA is 0.32 in a shear gradient which is large enough to cause some breakage. We will call such a shear gradient G_c. The dichroism value at G_c represents the average configuration of all the molecules in the solution only some of which are actually breaking. The value of $\langle \cos^2 \theta \rangle$ is thus 0.76 and the most probable end-to-end distance of the DNA is 11 μ. (The contour length of $\lambda b_2 b_5 c$ DNA is 12.8 μ.) We therefore used 5.5 μ as the value of the constant $\rho G_c b^3/kT$ to construct Figure 12.

We think the behavior of the dumbbell described by Eq. (79)

and plotted in Figure 12 is probably indicative of the behavior of the real system. One of the features which makes it especially appealing is demonstrated by Figure 13. In this figure, the value of ψ at x_c is plotted versus time. The value of x_c is taken as $\rho G_c b^3/kT$ plus 2b. We consider the instantaneous breakage rate to be proportional to $\psi(x_c, t)$. Figure 13 shows that while steady state breakage is achieved by the time the DNA exits from the 25 cm capillary, a substantial portion of the passage time is required to establish the steady rate. The time required is 2 or 3 times the relaxation time constant of 0.03 sec.

This feature of the model correlates very well with the experiments performed with capillaries of different lengths. In those experiments we saw that multiplying the residence time by 3.5 had the effect of multiplying the breakage rate per pass by 7. In the model we see the probable reason for this result. For the short capillary about half the residence time is required to set up steady breakage. But for the 90 cm capillary, only about one-tenth the total residence time is needed to establish the steady state rate.

According to our model then, the breakage rates <u>per pass</u> in the two capillaries, which are proportional to areas under the curve in Figure 13, cannot be in the same proportion as the residence times. And the reason is that steady state breakage is not achieved in a time which is short with respect to the residence time of the shorter capillary. It should be noted that this conclusion is independent of the choice of x_c. The same basic feature of the model results when x_c

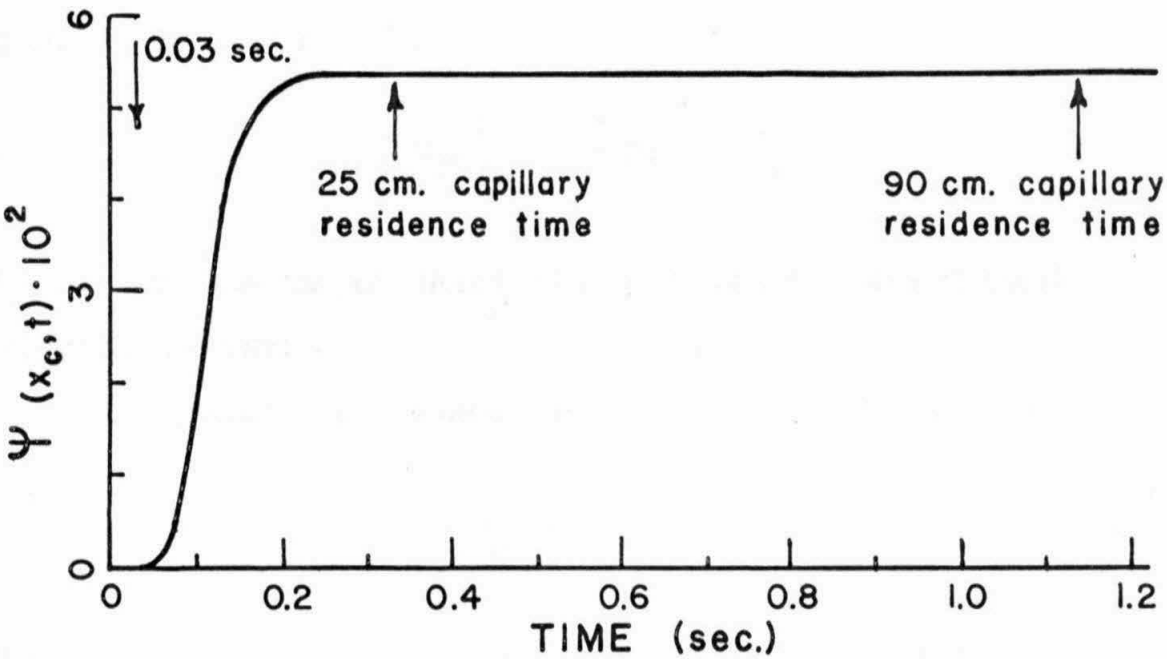

Fig. 13. The theoretical instantaneous breakage rate, $\psi(x_c, t)$, is plotted versus time. The value taken for x_c is $(\rho G_c b^3/kT + 2b)^c$ which corresponds to the point 13b on the abcissa of Fig. 12. The hydrodynamic relaxation time of $\lambda b_2 b_5 c$ DNA, 0.03 sec., is labelled in the figure as are the DNA residence times in the 25 cm. and 90 cm. capillaries.

is taken as $\rho G_c b^3/kT + nb$ where $n = 2, 3, 4, 5, \ldots$.

There are additional features of the dumbbell model which should be pointed out. (1) Our experiments demonstrate an inverse proportionality between breakage rate and viscosity. (2) We also observed the breakage rate to be extremely sensitive to the shear gradient. In fact, we found

$$\left.\frac{d\ \ell n\, k}{d\ \ell n\, G}\right)_{25°C} = 15 \tag{83}$$

We will now show that our dumbbell model is consistent with these experimental results.

The equation of motion of the dumbbell end [from Eq. (71)] is

$$\frac{dx}{dt} = Gb - \frac{kT}{\rho b^2} x - \frac{kT}{\rho} \frac{\partial\ \ell n\, \psi}{\partial x} \tag{84}$$

in which Gb has been substituted for the relative fluid velocity, v_f. The flux of molecules passing through some extension x is $\psi\, dx/dt$. Using the symbol F for the flux, we write

$$F(x, t) = Gb\psi - \frac{kT}{\rho b^2} x\, \psi - \frac{kT}{\rho} \frac{\partial \psi}{\partial x} \tag{85}$$

In our formulation of the dumbbell model, we stipulated that when the dumbbell reached a certain critical extension, x_c, it would break. At x_c then, $\psi = 0$ and the flux is

$$F(x_c, t) = -\frac{kT}{\rho} \frac{\partial \psi}{\partial x} \tag{86}$$

We assume that in the steady state $\partial\psi/\partial x$ is dependent on ηG but not on η. This is analogous to the kinetic model in which the rate of formation of extended random coils (B) is a ratio of rate constants and depends on ηG not η. Thus in this picture, the dumbbell model has an inverse relationship between the breakage rate, represented here by $F(x_c, t)$, and the frictional coefficient, ρ, which contains a viscosity factor.

Now, using Eq. (85) we can show the dumbbell model also has a reasonable dependence of breakage rate on shear gradient. The quantity we wish to evaluate and compare with the experimental result of Eq. (83) is $d\,\ell n\, F_{ss}(x_c)/d\,\ell n\, G$ where the subscript ss stands for steady state. From Eq. (85),

$$-\left(\frac{\rho}{kT}\right) F_{ss}(x) = \frac{\partial\psi}{\partial x} + \left(\frac{x}{b^2} - \frac{\rho G b}{kT}\right)\psi \tag{87}$$

which has the general solution

$$\psi(x) = Be^{-\frac{b^2}{2}\left(\frac{x}{b^2} - \frac{\rho G b}{kT}\right)^2} - e^{-\frac{b^2}{2}\left(\frac{x}{b^2} - \frac{\rho G b}{kT}\right)^2} \int_{x_1}^{x} \frac{\rho}{kT} F_{ss}(x)\, e^{\frac{b^2}{2}\left(\frac{z}{b^2} - \frac{\rho G b}{kT}\right)^2} dz \tag{88}$$

where the constant B depends on the value chosen for the arbitrary reference point, x_1. If we let $x_1 = \rho G b^3/kT$, and $\psi(x_1) = 1/\sqrt{2\pi}$ then $B = 1/\sqrt{2\pi}$.

We wish to evaluate $F_{ss}(x)$ at x_c and we have stipulated that $\psi = 0$ there. Thus

$$F_{ss}(x_c) = \frac{\sqrt{2\pi}\,kT}{\rho} \Bigg/ \int_{\frac{\rho Gb^3}{kT}}^{x_c} e^{\frac{b^2}{2}\left(\frac{z}{b^2} - \frac{\rho Gb}{kT}\right)^2} dz \tag{89}$$

By taking the natural logarithm of both sides of Eq. (89) and differentiating with respect to $\rho Gb^3/kT$, we obtain

$$\frac{d\,\ell n\, F_{ss}(x_c)}{d\left(\frac{\rho Gb^3}{kT}\right)} = 1 \Bigg/ \int_{\frac{\rho Gb^3}{kT}}^{x_c} e^{\frac{b^2}{2}\left(\frac{z}{b^2} - \frac{\rho Gb}{kT}\right)} dz + \frac{\int_{\frac{\rho Gb^3}{kT}}^{x_c} b^2\left(\frac{z}{b^2} - \frac{\rho Gb}{kT}\right) e^{\frac{b^2}{2}\left(\frac{z}{b^2} - \frac{\rho Gb}{kT}\right)^2} dz}{\int_{\frac{\rho Gb^3}{kT}}^{x_c} e^{\frac{b^2}{2}\left(\frac{z}{b^2} - \frac{\rho Gb}{kT}\right)^2} dz} \tag{90}$$

which may be written in a more tractable form by using the equality of Eq. (89).

$$\frac{d\,\ell n\, F_{ss}(x_c)}{d\left(\frac{\rho Gb^3}{kT}\right)} = \frac{\rho}{\sqrt{2\pi}\,kT} F_{ss}(x_c) + \frac{\rho}{\sqrt{2\pi}\,kT} F_{ss}(x_c)\left[e^{\frac{b^2}{2}\left(\frac{x_c}{b^2} - \frac{\rho Gb^2}{kT}\right)^2} - 1\right] \tag{91}$$

Or

$$\frac{d\,\ell n\,F_{ss}(x_c)}{d\,\ell n\,G} = \frac{\rho^2 b^3 G}{\sqrt{2\pi}\,(kT)^2}\,F_{ss}(x_c)\,e^{\frac{1}{2}\left(\frac{x_c}{b} - \frac{\rho G b^2}{kT}\right)^2} \tag{92}$$

Again making use of Eq. (89),

$$\frac{d\,\ell n\,F_{ss}(x_c)}{d\,\ell n\,G} = \frac{\frac{\rho b^3 G}{kT}\,e^{\frac{1}{2}\left(\frac{x_c}{b} - \frac{\rho G b^2}{kT}\right)^2}}{\int_{\frac{\rho G b^3}{kT}}^{x_c} e^{\frac{b^2}{2}\left(\frac{z}{b^2} - \frac{\rho G b}{kT}\right)^2} dz} \tag{93}$$

It now remains to evaluate the integral in the denominator of Eq. (93). We can simplify notation somewhat by taking the value $5.5\,\mu$ for the constant $\rho G b^3/kT$. This value was obtained for use in connection with Eq. (79) which is not strictly applicable here. However, it seems reasonable to use this value in light of the similarity between the solutions given by Eqs. (79) and (88). Since $b = 0.5\,\mu$,

$$\frac{\rho G b^3}{kT} = 11b$$

and

$$x_c = (11+n)b \qquad n = 2, 3, 4, \ldots$$

The integral we wish to evaluate is

$$\int_{11b}^{(11+n)b} e^{\frac{1}{2}\left(\frac{z}{b} - 11\right)^2} dz$$

A method for evaluating this integral is given in Appendix F. It is shown there that its value is approximately $b\, e^{n^2/2}/n$. Thus

$$\frac{d\, \ell n\, F_{ss}(x_c)}{d\, \ell n\, G} \approx \frac{n\rho G b^2}{kT} = 11n \qquad (94)$$

This calculation agrees quite nicely with the experimental result of Eq. (83) for values of n between 1 and 2. It shows that the dumbbell model we formulated has the same relationship between breakage rate and shear gradient as is observed in our experiments with DNA.

The usefulness of the theoretical model we have just discussed was mainly to show how our experimental results concerning capillary length arose. It assumes the rate determining step for shear breakage is in fact the rate DNA unfolds in the presence of a velocity gradient. The evidence supporting this assumption was discussed in the preceding section (Temperature and Viscosity Effects). The effect of residence time on breakage rate cannot itself confirm the nature of the rate limiting step. Were solvolysis of carbon-oxygen bonds rate determining, we might still observe similar residence time effects.

Conclusion

Our original approach to hydrodynamic shear breakage of native DNA was based on the hypothesis that breakage was probably a mechanically assisted hydrolysis reaction. We set out to demonstrate the existence of a temperature coefficient for breakage at constant shear stress. The temperature coefficient we found however did not

arise from the influence of temperature on a thermal hydrolysis reaction. We observed that at constant shear stress, the variation of solvent viscosity with temperature has a very marked effect on the rate of breakage. Our data show that the rate determining step for native DNA shear breakage is the viscosity limited rate of segmental diffusion of random coil molecules to extended configurations.

We have presented a kinetic model for DNA breakage whose main feature is that the rate of breakage is determined by the rate at which average extended random coil molecules in a liquid velocity gradient unfold to exceptionally extended configurations. The speed of this unfolding maneuver is limited by the speed at which segments of the DNA molecule can move through the solution and is therefore inversely porportional to the solution's viscosity. This model explains the viscosity effects observed experimentally. It qualitatively explains the self-protection effects for shear breakage at concentrations where the hydrodynamic interaction effects for unextended molecules are small. The oversimplified quantitative dumbbell model gives a reasonable prediction for the effects of shear stress, ηG. The theory and experiments presented here provide a firm foundation for further experimental and theoretical work.

REFERENCES

1. O. L. Forgacs and S. G. Mason, J. Colloid Sci., 14, 473 (1959).
2. P. Davison, Proc. Natl. Acad. Sci., 45, 1560 (1959).
3. A. D. Hershey and E. Burgi, J. Mol. Biol., 2, 143 (1960).
4. C. Levinthal and P. Davison, J. Mol. Biol., 3, 674 (1961).
5. R. E. Harrington and B. H. Zimm, J. Phys. Chem., 69, 161 (1965).
6. P. Davison and D. Freifelder, J. Mol. Biol., 16, 490 (1966).
7. D. Freifelder and P. Davison, Biophys. J., 2, 235 (1962).
8. L. F. Cavelieri and B. H. Rosenberg, J. Amer. Chem. Soc., 81, 5136 (1959).
9. E. Burgi and A. D. Hershey, J. Mol. Biol., 4, 313 (1962).
10. E. Burgi and A. D. Hershey, J. Mol. Biol., 3, 458 (1961).
11. I. Rubenstein, C. A. Thomas, and A. D. Hershey, Proc. Natl. Acad. Sci., 47, 1113 (1961).
12. H. S Rosenkranz and A. Bendich, J. Amer. Chem. Soc., 82, 3198 (1960).
13. P. Doty, B. B. McGill, and S. Rice, Proc. Natl. Acad. Sci., 44, 432 (1958).
14. R. E. Harrington, J. Polymer Sci. [A], 4, 489 (1966).
15. O. C. Richards and P. D. Boyer, J. Mol. Biol., 11, 327 (1965).
16. C. C. Richardson and B. Weiss, J. Gen. Physiol., 49, 81 (1966).
17. G. Barr, A Monograph of Viscometry, Oxford University Press, London (1931).

18. J. D. Mandell and A. D. Hershey, Anal. Biochem., 1, 66 (1960).

19. R. W. Davis, M. Simon, and N. Davidson, Methods in Enzymology, Academic Press, New York (1969).

20. D. M. Crothers and B. H. Zimm, J. Mol. Biol., 12, 525 (1965).

21. J. Vinograd and R. Bruner, Biopolymers, 4, 131 (1966).

22. C. S. Lee, personal communication.

23. If this procedure had been carried out at pH 8, very few single strand breaks would have been introduced. Norman Davidson, personal communication, 1970.

24. P. R. Callis and N. Davidson, Biopolymers, 7, 335 (1969).

25. P. R. Callis and N. Davidson, Biopolymers, 8, 379 (1969).

26. F. F. H. Yew and N. Davidson, Biopolymers, 6, 659 (1968).

27. M. Selin and P. Leduc, Comptes Rendus, 251, 1520 (1960).

28. W. F. Dove and N. Davidson, J. Mol. Biol., 5, 467 (1962).

29. V. W. Kuhn and F. Grün, Kolloid Zeitschrift, 101, 248 (1942).

APPENDIX A

Shear Breakage Apparatus

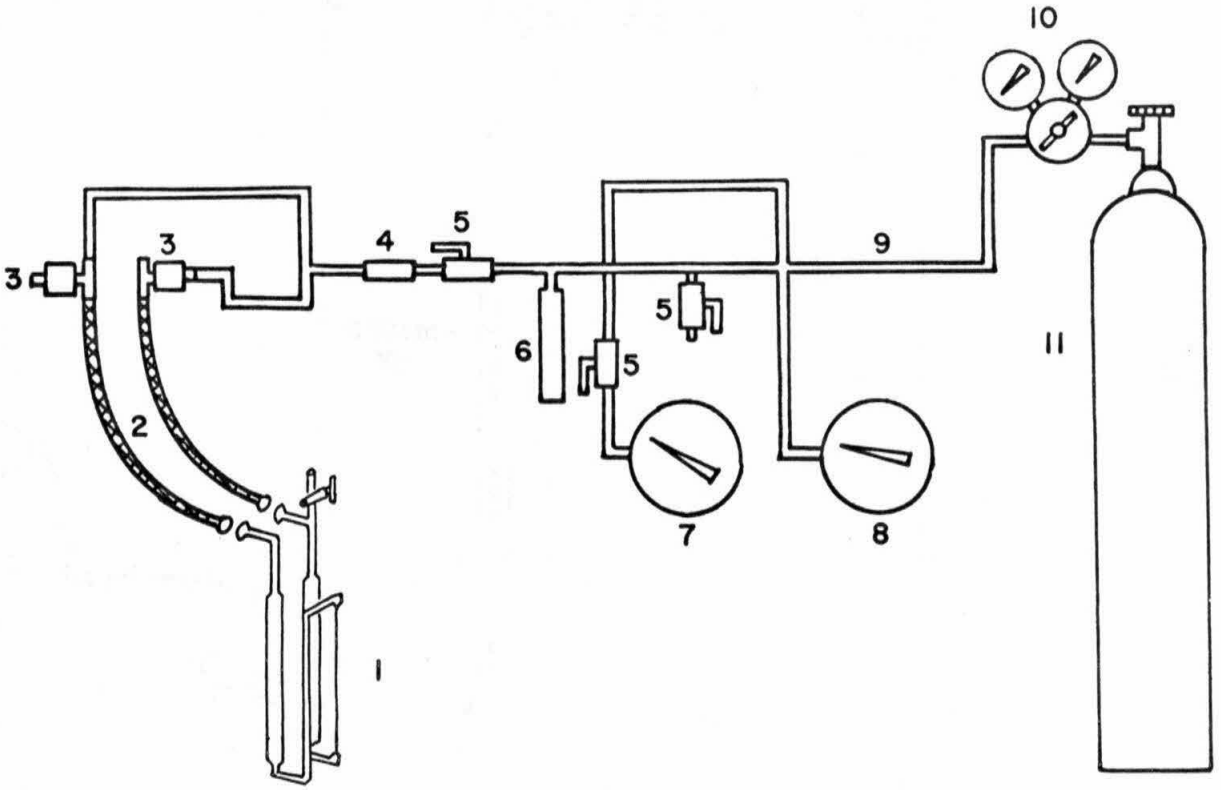

Fig. A1. Schematic drawing of the shear breakage apparatus. Photoelectric control units (not shown) are model M310 from Donner Electronics, Inc., Melrose, Mass. The capillary is normally immersed in a constant temperature water bath.

1. Pyrex capillary fitted with Teflon stopcock.
2. Flexible stainless steel tubing, 1/4".
3. Hoke solenoid three-way valves.
4. Hoke 540 series micron filter (stainless steel).
5. Hoke cam closing toggle valves.
6. Ballast (stainless steel pipe, 1" × 12").
7. Marshalltown Permaguage (0-100 psi).
8. Marshalltown Permaguage (0-300 psi).
9. 1/4" stainless steel tubing.
10. Harris multi-stage pressure regulator.
11. Nitrogen tank.

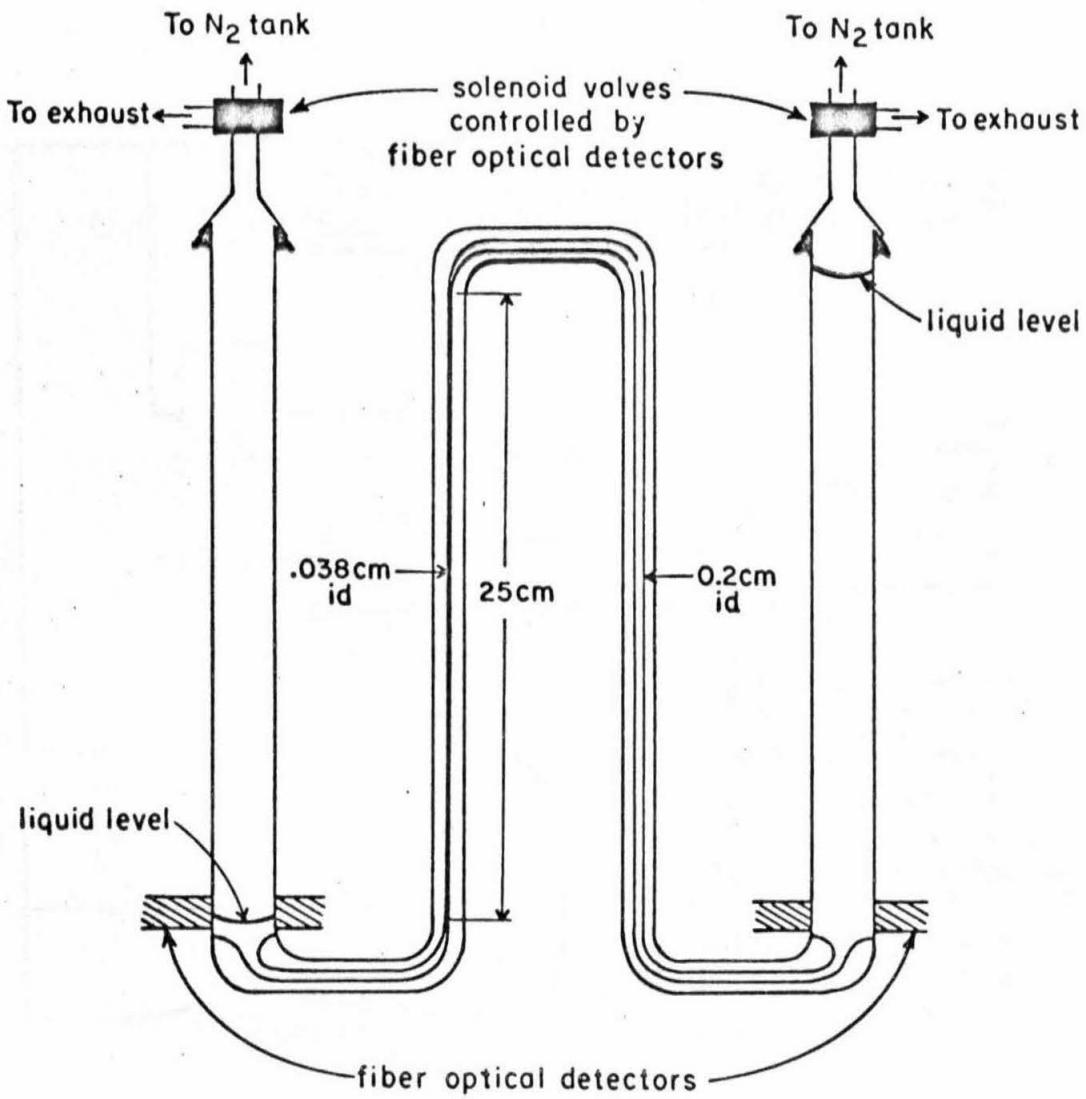

Fig. A2. Schematic drawing of a 25 cm. capillary (capillary #1 in Table I). Note that the liquid level in the left-hand reservoir is the lowest level reached by the liquid. At the position shown, the meniscus intersects the light beam between the fiber optical detectors (called optic fiber scanners or light pipes in the text). The volume of solution between this liquid level and the capillary and the corresponding volume between the capillary and the right-hand light pipes make up the dead volume referred to in the Experimental section and Table I. The capillary connects to the flexible stainless tubing (see Fig. A1) by means of 12/3 ball joints. The female ball joints are machined from stainless steel and silver soldered to the flexible tubing. An O-ring makes a seal between the glass and metal surfaces.

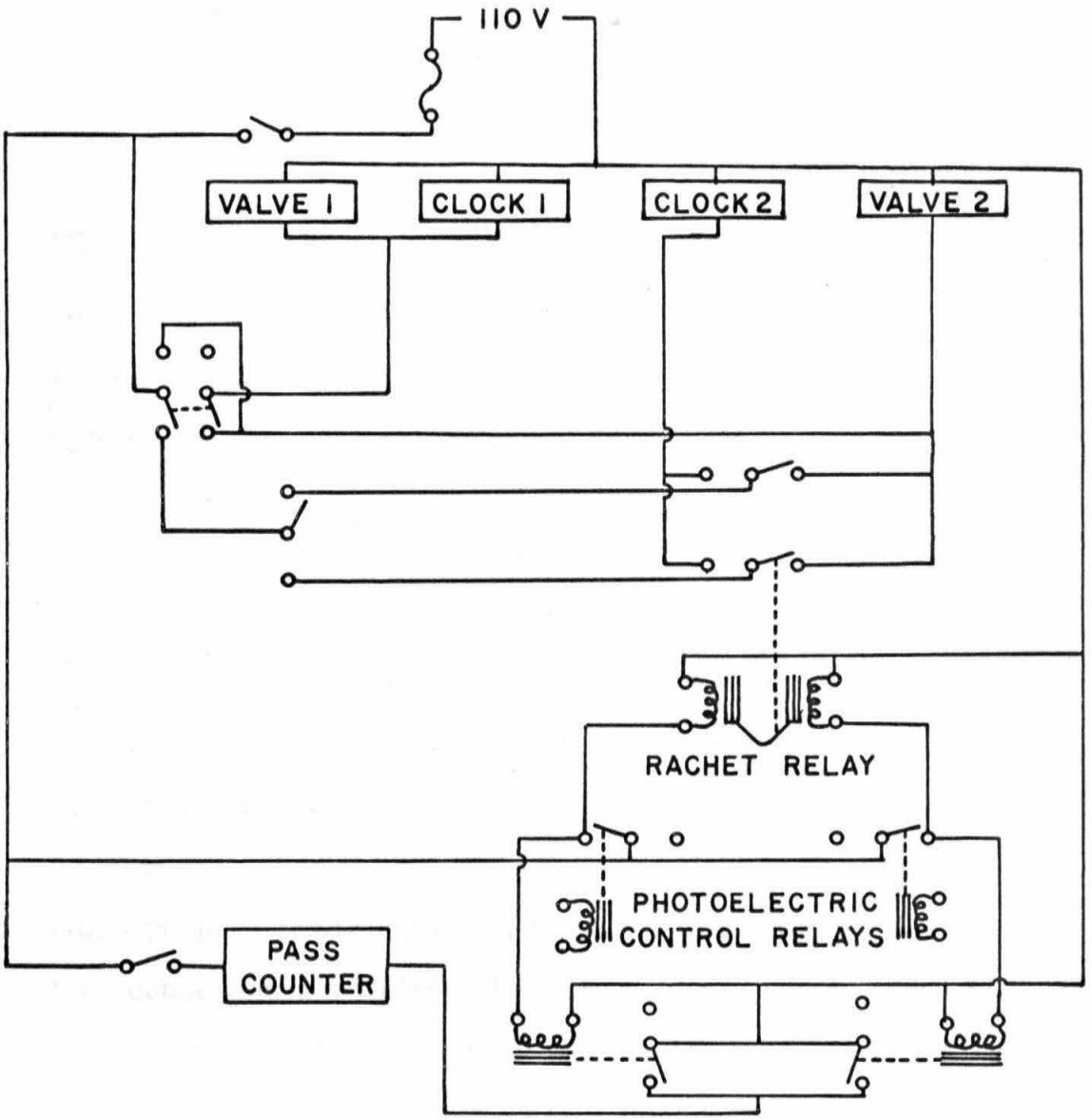

Fig. A3. Shear apparatus wiring diagram. A photoelectric control relay is activated whenever a meniscus comes between the light pipes of the appropriate reservoir. The valves operate as follows:

Valve	Energized	De-energized
1	Connects capillary to pressurized N_2	Connects capillary to atmosphere
2	Connects capillary to atmosphere	Connects capillary to pressurized N_2

APPENDIX B

Preparation of $\lambda b_2 b_5 c$ DNA

Lambda Phage Growth:

1) Grow an overnight culture (10 ml) of plating bacteria, E. coli C 600, in tryptone broth (containing 20 μg thiamine/ml) at 37°C.
2) Spin the plating bacteria down and resuspend in 100 ml TMG.

TMG: 0.01 F Tris pH 7.4
0.01 F $MgSO_4$
0.1% gelatin (w/v)

3) Plate your phage stock so that the plaques are well separated. (Plating procedure and recipes are given below.)
4) After plaques have developed, put 1 ml chloroform on the plate and swirl it around so it contacts the entire plate surface.
5) Dig a plaque out with an innoculation needle and drop it into a test tube containing 5 ml TMG. Let stand for at least two hours. Addition of a drop or two of chloroform is advisable if the test tube is left at room temperature for several hours.
6) Plate this phage suspension on three-to-five more agar plates, this time planning for 500 to 2000 plaques per plate.
7) When these plates have developed to the point at which the plaques are just about touching (but not to the point at which the plate is clear), add 1 ml chloroform and swirl around as before to cover all the bacteria.
8) Add 5 ml TMG to each plate and let stand for two or more hours (occasionally agitate).

9) Retrieve the phage suspension by pouring the TMG into the plate cover and sucking it up with a pipet. This is the plate stock with which the main culture will be innoculated. Store it over a little chloroform at 4°C. Its titer should be determined.

10) Grow an overnight culture of E. coli K12 W3110 in tryptone broth (37°C).

11) Prepare the main culture medium, Bowman-Lee Broth (BLB), consisting of:

1.5% (w/v) tryptone
0.5% (w/v) yeast extract
0.5% (w/v) NaCl
20 ml 10% (w/v) glucose per liter
5 ml 1 F $MgSO_4$ per liter
0.2 ml 0.5 F $CaCl_2$ per liter

The latter three solutions should be autoclaved separate from each other and separate from the first three. The pH of the medium, when mixed, should be 7.

12) Good aeration is important during phage growth. Suitable culture containers can be constructed out of 500 ml or 1 liter mixing cylinders. Use gas dispersion tubes to introduce the air supply. Add 10 ml of the overnight culture to 1 liter BLB. Grow the bacteria to a concentration of 2×10^8 bacteria/ml (37°C). Add antifoam as necessary to prevent overflow.

13) Infect the bacteria with phage from the plate stock at a multiplicity of infection of 1 phage/20 bacteria.

14) Follow the bacterial growth by turbidity or bacterial count. Monitor the pH. Add NaOH as required to keep the medium at

pH 7. The first lysis occurs in about one hour, the second an hour later. If conditions are right, one observes a significant decrease in turbidity (A_{600}) two hours after phage infection. When the turbidity begins to increase again, add 15 ml chloroform per liter of medium and continue aeration 15 minutes. Then chill the culture and store at 4°C.

[It is not unusual to observe constant turbidity readings two hours after infection instead of a sudden decrease. Add the chloroform after 15 minutes of constant turbidity readings, aerate and chill. If the turbidity drops as low as $A_{600} = 0.1$ one hour after infection you may have grown phage T1.]

Useful tips:

E. coli C600 works better than E. coli K12 W3110 on the surface of agar plates. The W3110 strain is superior to C600 in a liquid medium.

λ bacteriophage sometimes has trouble adsorbing to bacteria in their log phase. Two procedures prevent the problem. Either (a) infect the bacteria when they are suspended in TMG; (b) use a super rich medium such as BLB.

One normal sized λ phage plaque contains about 5×10^8 phage.

$$10^{12} \lambda \text{ phage} \approx 50 \ \mu g \text{ of DNA}$$

Antifoam = proplyene glycol monolaurate, obtainable from Armour Industries, 401 North Wabash Ave., Chicago, Ill. 60690.

Plating technique:

Add $\frac{1}{2}$ ml of the plating bacteria as prepared in steps 1 and 2 above to a 5 ml test tube (room temperature). Add 0.1 ml of the phage

solution you wish to plate. Wait 10 minutes. Add 2.5 ml of top agar (45°C), mix and quickly pour onto agar plate. Swirl plate slightly so liquid agar covers the whole surface.

Bottom Agar:	Tryptone	10 g
	Agar	10 g
	NaCl	5 g
	Water	1 ℓ

Autoclave and cool to 45°-50°C. Pour about 30 cc/plate. Make plates at least 24 hours before intended use.

Top Agar:	Tryptone	1.0 g
	Agar	0.65 g
	NaCl	0.5 g
	Water	100 ml

Bacterial Cultures:

Grow cells in 10 ml tryptone broth or any convenient medium to a concentration of 10^8 bacteria/ml.

Add 1 ml of this culture to 10 ml fresh media and continue growing for 30 minutes.

Add 2.5 ml glycerin and be sure to mix it well. Let stand for 10 minutes and mix again.

Freeze the preparation in a convenient container.

Innoculate larger cultures directly from this stock. A portion of the frozen stock is thawed as required.

Phage yields have been substantially increased by using stocks derived from a single bacteria. Plate your bacterial stock. Select

6-10 colonies and grow phage separately on each (50 ml cultures). The colony which performs best is kept according to the procedure above for future phage production.

Tryptone broth:

Tryptone	10 g
NaCl	5 g
Water	1 liter

Adjust pH to 7.

Phage Purification:

1) After chloroform treatment, chill the phage culture, take a sample for assay and spin down the bacterial debris (Sorvall GSA rotor, 7K, 10 minutes).
2) To each liter of supernatent add 28 g NaCl, 360 ml of a solution containing 30% (w/v) polyethylene glycol and 3.4 ml of a solution containing 20% (w/v) dextran sodium sulfate. Mix well and let stand overnight in a separatory funnel at 4°C.
3) Centrifuge the lower white phase in the Sorvall SS-34 rotor, 3K, 15 minutes. Lift out the "cake" which forms at the interface of the two phases (or remove the upper and lower phases from around it).
4) Resuspend the cake in 0.01 F Tris pH 7.4, 0.01 F $MgSO_4$. Add dextran sulfate to give $\geq$ 1% and add 0.15 by volume 3M KCl. Let stand two hours.

5) Centrifuge in Sorval rotor SS-34, 3 K, 10 minutes. Bluish supernatent is phage.
6) Pellet phage in SW 25.1 rotor, 22 K, 2 hours. Resuspend in TMG to make a total volume of 6 ml.
7) Band this phage in a buoyant cesium chloride density gradient in a SW 50 rotor, 40 K, for no less than 48 hours. (The density of $\lambda b_2 b_5 c$ phage is 1.48 g/cc.) It is helpful to have only 4 ml of phage in each of the SW 50 rotor buckets. Add bayol to prevent collapse of the cellulose nitrate tubes.
8) Collect the phage from a hole punched in the side of the cellulose nitrate tubes. Phage are conveniently stored in this CsCl solution. Alternatively, dialyze against TMG and store the phage over chloroform.

DNA Extraction:

1) Distill 100 ml or so phenol under nitrogen. Saturate it with the following buffer overnight at 4 °C.

0.1 F NaCl
0.1 F phosphate pH = 8
0.01 F EDTA

2) The phage suspension to be extracted should have at least as high a salt concentration as the buffer with which the phenol is equilibrated.
3) Add an equal volume of phenol to the phage suspension. Gently rock the two phases back and forth for 5-10 minutes. The extraction procedure should be done at 4 °C.

4) Centrifuge the phage briefly in a clinical centrifuge to help separate the phases.
5) Discard the lower, phenolic phase and repeat steps 3 and 4.
6) Now perform at least five (diethyl) ether extractions. Discard the upper, ether phase each time.
7) Dialyze the DNA against two changes of 0.1 F EDTA, pH 8.
8) Dialyze the DNA against four or five changes of the buffer of your choice.

APPENDIX C

Shear Breakage Experiments

Capillary*	[DNA] (μg/ml)	Buffer	T (°C)	P (psi)	V (ml/sec)	G_m (sec^{-1})	η (centi-poise)	Re	$\langle P \rangle$
2	7.5	PE	25	43	0.549	99,616	0.8937	2036	1×10^{-3}
2	7.5	PE	25	45	0.568	103,000	0.8937	2106	$2.6 \times 10^{-3} \pm 5.4 \times 10^{-4}$
2	7.5	PE	1	95	- - -	- - -	1.732	- -	$2.5 \times 10^{-3} \pm 1.9 \times 10^{-4}$
2	7.5	PE	20	45	0.515	93,400	1.005	1700	$5.5 \times 10^{-4} \pm 5.3 \times 10^{-5}$
2	7.5	PE	30	45	- - -	- - -	- - -	- -	$7.3 \times 10^{-3} \pm 9.8 \times 10^{-4}$
2	7.5	PE	5	88	0.685	124,000	1.519	1500	$5.5 \times 10^{-3} \pm 7.8 \times 10^{-4}$
2	7.5	PE	4	88	0.666	121,000	1.567	1412	$9.0 \times 10^{-4} \pm 3.0 \times 10^{-4}$
2	7.5	PE	10	72	0.636	115,000	1.308	1616	$4.6 \times 10^{-3} \pm 6.0 \times 10^{-4}$
2	7.5	PE	7	72	- - -	- - -	- - -	- -	no breakage
2	7.5	PE	15	62	0.617	112,000	1.140	1798	$3.7 \times 10^{-3} \pm 4.1 \times 10^{-4}$
2	7.5	PE	10	62	0.550	100,000	1.308	1398	$1.0 \times 10^{-4} \pm 1.7 \times 10^{-5}$
2	7.5	PE/6.3	25	45	0.575	104,000	0.8937	2132	$2.3 \times 10^{-3} \pm 3.2 \times 10^{-4}$
2	7.5	PE†	25	90	0.642	116,000	1.732†	1332	$9.9 \times 10^{-4} \pm 2.4 \times 10^{-4}$
2	7.5	PE	10	67	0.593	108,000	1.308	1507	$1.3 \times 10^{-3} \pm 3.0 \times 10^{-4}$
2	7.5	PE	25	40	0.510	92,300	0.8937	1891	$7.9 \times 10^{-4} \pm 2.1 \times 10^{-4}$

Capillary*	[DNA] (μg/ml)	Buffer	T (°C)	P (psi)	V (ml/sec)	G_m (sec^{-1})	η (centi-poise)	Re	$\langle P \rangle$
2	7.5	PE	25	35	0.448	81,200	0.8937	1661	$9.7 \times 10^{-5} \pm 5 \times 10^{-6}$
3	7.5	PE	25	168	0.648	118,000	0.8937	2301	$1.7 \times 10^{-2} \pm 3.1 \times 10^{-3}$
3	7.5	PE	25	131	0.510	92,300	0.8937	1811	$7.7 \times 10^{-4} \pm 1.1 \times 10^{-4}$
2	7.5	PE	25	45	0.568	103,000	0.8937	2106	$2.5 \times 10^{-3} \pm 4.3 \times 10^{-4}$
1	5.0	E	25	18-26	- - -	- - -	0.8937	- -	breakage at 24 psi (100 passes)
1	7.5	E	25	24-50	- - -	- - -	0.8937	- -	breakage at 38 psi (100 passes)
1	5.0	E	25	18-48	- - -	- - -	0.8937	- -	breakage at 24 psi (100 passes)
1	5.0	PE	25	16-42	- - -	- - -	0.8937	- -	breakage at 34 psi (100 passes)
1	0.5	PE	25	24-38	- - -	- - -	0.8937	- -	breakage at 30 psi (100 passes)
1	2.5	PE	25	10-40	- - -	- - -	0.8937	- -	breakage at 32 psi (100 passes)
1	3.75	PE	25	28-40	- - -	- - -	0.8937	- -	breakage at 32 psi (100 passes)
1	5.9	PE	25	18-40	- - -	- - -	0.8937	- -	breakage at 34 psi (100 passes)
2	2.5	PE	25	36	- - -	- - -	0.8937	- -	experiments employing dichroism
2	2.5	PE	25	38	- - -	- - -	0.8937	- -	
2	2.5	PE	25	40	- - -	- - -	0.8937	- -	

Capillary*	[DNA] (μg/ml)	Buffer	T (°C)	P (psi)	V (ml/sec)	G_m (sec^{-1})	η (centi-poise)	Re	⟨P⟩
2	2.5	PE	25	37	- - -	- - -	0.8937	- -	⎫
2	7.5	PE	25	10-30	- - -	- - -	0.8937	- -	Hershey circles don't break psi ≤ 30
2	7.5	PE	25	30-38	- - -	- - -	0.8937	- -	Hershey circles break about 32 psi
2	7.5	PE	25	40	0.510	92,200	0.8937	1891	

*See Table I for capillary specifications.

†The buffer here is: 0.086 F NaCl
0.0086 F EDTA
0.0043 F phosphate
20.1% (w/v) sucrose
pH = 7.0

[DNA] means DNA concentration

T = temperature

P = nitrogen gas driving pressure

V = volume flow rate

G_m = maximum shear gradient

η = viscosity

Re = Reynolds' number

⟨P⟩ = probability of breakage per pass (error interval is 95% confidence interval)

PE = phosphate EDTA buffer consisting of
0.1 F NaCl
0.01 F EDTA
0.005 F phosphate
pH = 7.0

E = EDTA buffer consisting of
0.1 F NaCl
0.01 F EDTA
pH = 7

APPENDIX D

Half-Molecule Molecular Weight Dispersion Measured by Band Velocity Sedimentation

Vinograd and Bruner present a method for analyzing the band shape in a velocity sedimentation experiment to determine the distribution of sedimentation coefficients it represents.* From the distribution of sedimentation coefficients, one may obtain a distribution of molecular weights. In the present work application of the method to a band of half-molecules could give the distribution of breakage point locations. But DNA concentrations normally used in this work, for both breakage and velocity sedimentation, are low and some of the more dilute components of a molecular weight distribution are lost in the noise of the centrifuge's scanning system. Thus the method of choice here is electron microscopy which can detect all the components of the distribution.

The object of this appendix is to show that within the limits of the centrifuge detection system there is good agreement between the electron microscopy results and those obtained from the Vinograd-Bruner method.

We begin with analysis of a band of whole $\lambda b_2 b_5 c$ DNA molecules (molecular weight 25×10^6 daltons). The concentration versus radius curve obtained directly from the centrifuge is shown in Figure D(a)

---

*J. Vinograd and R. Bruner, Biopolymers, 4, 131 (1966).

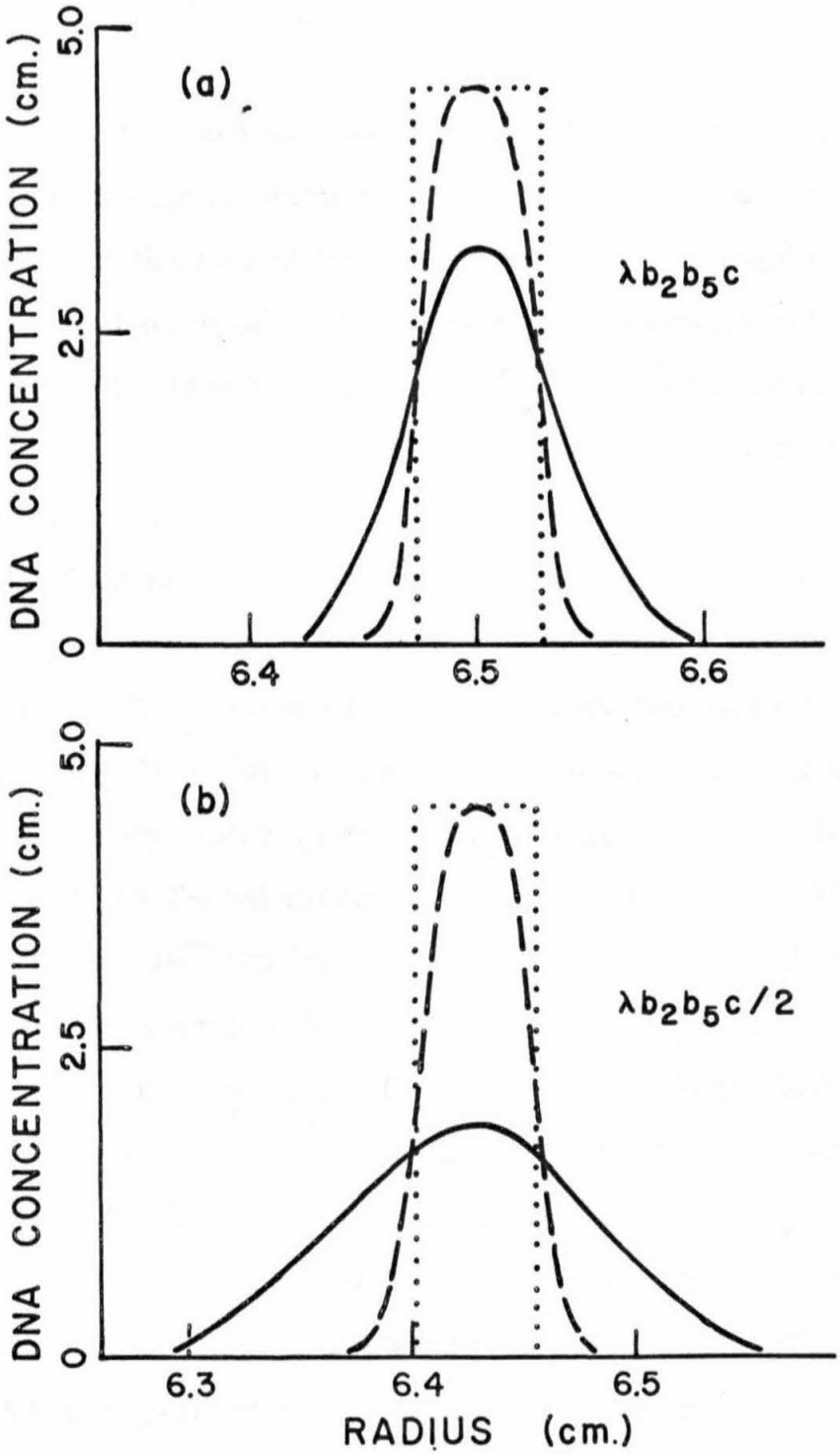

Fig. D. Plots of concentration versus distance from the center of rotation in band velocity sedimentations of whole and half $\lambda b_2 b_5 c$ molecules. The concentration units derive from the height of the DNA peaks as they appeared on scanner tracings.

(solid curve). The DNA has sedimented 6360 sec and $\omega^2 = 1.08 \times 10^7$ sec^{-2}. With the experimental curve are two theoretical curves representing the contributions of the inhomogeneous centrifugal field and diffusion to the band width. The DNA band at the beginning of the run is in the form of a lamella 0.5 mm thick. If this lamella of whole molecules were allowed to sediment undisturbed by diffusion and convection or other irregularities, it would have the shape of the dotted outline in Figure D(a). It is thicker than 0.5 mm (actually 0.58 mm thick) because the leading edge always experiences a greater centrifugal force than the trailing edge and therefore sediments faster.

If this widened lamella is now allowed to diffuse for 6360 sec. undisturbed by the centrifugal field and irregularities, it will have the appearance of the dashed curve in the figure. This curve was calculated using 5.5×10^{-9} cm^2/sec for the diffusion coefficient for $\lambda b_2 b_5 c$ DNA; it approximates the shape of a real band under ideal conditions.

We have assumed that the contributions to band spreading from the inhomogeneous field and diffusion are uncoupled whereas in fact they are not. As the band diffuses the leading and trailing edges get farther apart and will experience an even greater disparity in centrifugal force than we have pictured here. Thus the theoretical Gaussian band shown is slightly narrower than a real band should be.

The difference between the experimentally observed band width and the calculated one is much larger than the error introduced by our approximations. The cause of the difference is a combination of imperfections. These include: imperfect layering of DNA on the bulk

solution, variation of sedimentation velocity with DNA concentration, restricted diffusion at the meniscus, convection, and imperfections in the centrifuge apparatus. We will take the observed variance between the experimental (solid) and theoretical (dashed) curves in Figure D(a) as a measure of these imperfections. We will subtract the spreading represented there from all DNA bands observed under similar conditions in order to estimate the spreading caused by other factors.

A distribution of sedimentation coefficients and therefore of molecular weight may be obtained if we convert the concentration versus radius plot of Figure D(a) to a concentration versus sedimentation coefficient curve using the relation

$$s(r) = \frac{1}{\omega^2 \Delta t} \ell n \, (r/r_a) \tag{1D}$$

where s is the sedimentation coefficient, ω is the angular velocity, Δt is the time interval, r_a is the initial radius and r is the final radius. Following Vinograd and Bruner, this curve is then divided into intervals of $\Delta s = 1.2$. The weight fraction of material having sedimentation coefficients between s and $s + \Delta s$ is

$$g(s) = \frac{c(s)\, e^{2s\omega^2(t-t_i)}}{\sum_{s=0}^{\infty} c(s)\, e^{2s\omega^2(t-t_i)}} \tag{2D}$$

where $c(s)$ is the mean concentration of material with sedimentation

coefficients between s and $s + \Delta s$. Table D lists the weight distribution of sedimentation coefficients calculated with Eq. (2D) and the associated molecular weight distribution.* For the experimental distribution, the weight average sedimentation coefficient, $\overline{s}_w^0$, is 21.4 S (S = 1 Svedberg) and the standard deviation, σ_s is 0.75S. The weight average molecular weight, $\overline{M}_w$, is 23.6×10^6 daltons and its standard deviation, σ_m, is 2×10^6 daltons. For the theoretical curve, $\overline{s}_w^0$ = 21.2 S, σ_s = 0.7 S; $\overline{M}_w = 23.0 \times 10^6$ daltons, $\sigma_m = 1.7 \times 10^6$ daltons. The apparent variance in molecular weight due to imperfections in the system, $(\sigma'_m)^2$, is

$$(\sigma'_m)^2 = \sigma^2_m \text{(experimental)} - \sigma^2_m \text{(theoretical)}$$
$$= 1.2 \times 10^{12} \text{ daltons}^2$$

A half-molecule band is treated in an analogous way in Figure D(b) and Table D. Here the sedimentation time is 6740 sec (ω^2 is 1.08×10^7 sec^{-2}) and the diffusion coefficient is 8.6×10^{-9} cm^2/sec. For the experimental half molecule curve (solid line), $\overline{s}_w^0$ = 16.6 S, σ_s = 1.2 S; $\overline{M}_w = 12.5 \times 10^6$ daltons and $\sigma_m = 2.2 \times 10^6$ daltons. For the associated theoretical curve (dashed line) showing the effect of diffusion and inhomogeneous field only, $\overline{s}_w^0$ = 16.5 S, σ_s = 0.6 S; $\overline{M}_w = 12.5 \times 10^6$ daltons, $\sigma_m = 1.1 \times 10^6$ daltons. The difference between the molecular weight variances of the experimental and

---

*D. M. Crothers and B. H. Zimm, J. Mol. Biol., 12, 525 (1965).

Table D

Whole Molecules			Half Molecules		
g(s)	$\langle s^0 \rangle$ (Svedbergs)	$\langle M \rangle^*$ (daltons $\times 10^{-6}$)	g(s)	$\langle s^0 \rangle$ (Svedbergs)	$\langle M \rangle^*$ (daltons $\times 10^{-6}$)
Experimental			Experimental		
0.017	19.5	18.7	0.030	13.8	7.7
0.433	20.7	21.7	0.128	14.9	9.4
0.489	21.9	24.9	0.326	16.0	11.4
0.060	23.1	28.4	0.334	17.1	13.4
			0.158	18.2	15.7
			0.024	19.3	18.2
Theoretical			Theoretical		
0.565	20.6	21.5	0.512	16.0	11.5
0.435	21.9	25.0	0.488	17.1	13.6

*D. M. Crothers and B. H. Zimm, J. Mol. Biol., 12, 525 (1965).

theoretical curves is

$$(\sigma'_m)^2 = \sigma^2_m \text{ (experimental)} - \sigma^2_m \text{ (theoretical)}$$
$$= 3.88 \times 10^{12} \text{ daltons}^2$$

The portion of the band width we ascribe to molecular weight heterogeneity, Σ_m, is

$$\Sigma_m = [(\sigma'_m)^2 \text{ halves} - (\sigma'_m)^2/2 \text{ wholes}]^{\frac{1}{2}}$$
$$= 1.8 \times 10^6 \text{ daltons}$$

Thus the standard deviation in half-molecule molecular weight, 1.8×10^6 daltons, represents about $0.15\ \overline{M}_w$. In the Results section, we observed a standard deviation of $0.25\ \overline{M}_w$ based on electron microscopy data. As Figure 3 shows, a larger range of molecular weights was employed in the microscopy calculation than is detectable in the centrifuge. Table D lists molecular weights in the range $8 \times 10^6 \leq M \leq 18 \times 10^6$ daltons whereas Figure 3 shows molecules in the range $4 \times 10^6 \leq M \leq 22 \times 10^6$ daltons. If we use only that portion of the electronmicrograph histogram representing molecular weights from 8 to 18 million, we calculate the standard deviation to be $0.14\ \overline{M}_w$ which agrees nicely with the $0.15\ \overline{M}_w$ standard deviation derived from the centrifuge data.

APPENDIX E

Derivation of the R.M.S. End-to-End Distance of $\lambda b_2 b_5 c$ DNA in a Velocity Gradient Just Large Enough to Cause Breakage

From Kuhn and Grün,* the number of statistical segments in a polymer, N, is

$$N = \tfrac{1}{2} \int_0^{\pi} e^{\alpha} e^{\beta \cos\theta} \sin\theta \, d\theta$$

$$= \frac{e^{\alpha}}{\beta} \sinh\beta \qquad (1)$$

where α and β are Lagrange multipliers. The angle θ is the angle between each segment and a line drawn from one end of the polymer to the other. The end-to-end distance of the polymer, h, is

$$h = \int_0^{\pi} A \cos\theta \, e^{\alpha} e^{\beta \cos\theta} \sin\theta \, d\theta$$

$$= \frac{A e^{\alpha}}{\beta^2} (\beta \cosh\beta - \sinh\beta) \qquad (2)$$

The ratio of the end-to-end distance to the polymer's contour length is

$$\frac{h}{NA} = \coth\beta - \frac{1}{\beta} \qquad (3)$$

$$= L(\beta)$$

---

*W. Kuhn and F. Grün, Kolloid Zeitschriff, 101, 248 (1942).

where L stands for the Langevin function.

The product of N times the average square of $\cos\theta$ is

$$N\langle\cos^2\theta\rangle = \tfrac{1}{2}\int_0^{\pi} \cos^2\theta\, e^{\alpha} e^{\beta\cos\theta} \sin\theta\, d\theta$$

$$= \frac{e^{\alpha}}{\beta^3}\left[\beta^2 \sinh\beta - 2\beta\cosh\beta + 2\sinh\beta\right] \tag{4}$$

From Eqs. (1) and (4) we arrive at an expression for $\langle\cos^2\theta\rangle$,

$$\langle\cos^2\theta\rangle = 1 - \frac{2\coth\beta}{\beta} + \frac{2}{\beta^2} \tag{5}$$

This quantity may be written in terms of the ratio h/NA using Eq. (3).

$$\langle\cos^2\theta\rangle = 1 - \frac{2}{\beta}\left(\frac{h}{NA}\right) \tag{6}$$

Thus if we know $\langle\cos^2\theta\rangle$ we can calculate the value of β from Eq. (5). Knowing both $\langle\cos^2\theta\rangle$ and β we can calculate h/NA from Eq. (6).

Callis and Davidson* estimate the dichroism of $\lambda b_2 b_5 c$ DNA to be 0.32 when it is in a shear gradient just large enough to cause some breakage. From the relation between dichroism and $\langle\cos^2\theta\rangle$,

$$\frac{\Delta A}{A} = \tfrac{3}{4}\left[\langle\cos^2\theta\rangle - \tfrac{1}{3}\right] \tag{7}$$

---

*P. Callis and N. Davidson, Biopolymers, 7, 335 (1969).

we calculate $\langle \cos^2 \theta \rangle$ to be 0.76 for $\lambda b_2 b_5 c$ molecules in such a gradient. So, from Eq. (5), $\beta = 7.18$ and from Eq. (6), $h/NA = 0.86$. Taking 12.8 μ as the contour length for $\lambda b_2 b_5 c$ CNA, we arrive at 11 μ as the average end-to-end distance for these molecules.

APPENDIX F

Evaluation of the Integral: $\int_{11b}^{(11+n)b} e^{\frac{1}{2}(t/b - 11)^2}\, dt$

Let $y = t/b$; $dy = dt/b$

$$b \int_{11}^{11+n} e^{\frac{1}{2}(y - 11)^2}\, dy$$

Let $z = (11+n) - y$ (= upper limit - variable)

$$b \int_{o}^{n} e^{\frac{1}{2}(n - z)^2}\, dz$$

For small n, the quantity $e^{\frac{1}{2}(n - z)^2}$ may be fairly well approximated by $e^{\frac{1}{2}(n^2 - 2nz)}$. Thus the integral becomes

$$be^{n^2/2} \int_{o}^{n} e^{-nz}\, dz = \frac{be^{n^2/2}}{n} (1 - e^{-n^2})$$

Since $1 \gg e^{-n^2}$, we may ignore the second term in brackets above and conclude that

$$\int_{11b}^{(11+n)b} e^{\frac{1}{2}(t/b - 11)^2}\, dt \approx \frac{be^{n^2/2}}{n}$$

PLEASE NOTE:

Pages 117-155, Personal Letters relative to research and page 156, "Propositions", not available for microfilming.

UNIVERSITY MICROFILMS.